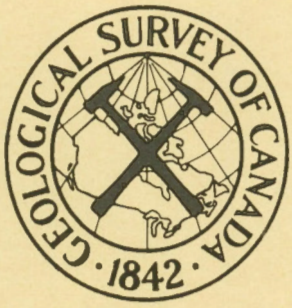

GEOLOGICAL
SURVEY
OF
CANADA

DEPARTMENT OF ENERGY,
MINES AND RESOURCES

PAPER 73-23

SEDIMENTATION AND MANGANESE CONCRETIONS IN A BRITISH COLUMBIA FIORD (JERVIS INLET)

R.D. Macdonald, J.W. Murray

GEOLOGICAL SURVEY
OF CANADA

PAPER 73-23

SEDIMENTATION AND MANGANESE CONCRETIONS IN A BRITISH COLUMBIA FIORD (JERVIS INLET)

R.D. Macdonald, J.W. Murray

DEPARTMENT OF ENERGY, MINES AND RESOURCES

Available by mail from *Information Canada*, Ottawa

from the Geological Survey of Canada
601 Booth St., Ottawa

and

Information Canada bookshops in

HALIFAX - 1687 Barrington Street
MONTREAL - 640 St. Catherine Street W.
OTTAWA - 171 Slater Street
TORONTO - 221 Yonge Street
WINNIPEG - 393 Portage Avenue
VANCOUVER - 800 Granville Street

or through your bookseller

Price: $3.00 Catalogue No. M44-73-23

Price subject to change without notice

Information Canada
Ottawa
1973

CONTENTS

Illustrations

Page

Appendices A and B

ABSTRACT

Manganese-iron oxide concretions are presently forming on a submarine ridge (Patrick Sill) in upper Jervis Inlet. The sedimentology and oceanography of Patrick Sill and the adjoining basins were studied to define the depositional environment.

The river at the inlet head is the principal source of sediment to the upper basin. The average grain size of surficial bottom sediments decreases uniformly with distance from source. The sediment distribution pattern within the lower basin differs markedly from that in the upper basin as there is no dominant source of material but rather, many localized sources.

Abundant shallow marine faunal remains found in deep water sediment samples indicate that sediments deposited as deltas off river and stream mouths periodically slump to the basin floors. Sedimentological and optical turbidity data for the upper basin can best be explained by slumping from the delta at the inlet head with the initiation of turbidity or density currents. Patrick Sill appears to create a downstream barrier to this flow.

The mineralogy of the bottom sediments indicates a granitic source. Upper Jervis Inlet is mapped as lying within a roof pendant of pre-batholithic rocks, mainly argillites. Thus, the sediments now being deposited are reworked glacial materials initially derived outside the present watershed.

Data suggest Patrick Sill is a bedrock feature mantled with Pleistocene glacial material. The accumulation rate of recent sediments on the sill is low, especially, in the medial depression. The manganese-iron oxide concretions, iron oxide crusts and glauconite-montmorillonoid pellets are forming only within this depression. The concretions are believed to form by precipitation of manganese-iron oxides on pebbles and cobbles lying at the sediment-water interface. The metal ions are mobile in the reducing environment of the underlying clayey-sand sediment but precipitate on contact with the oxygenating environment of the surficial sediments. The iron crusts are forming on extensive rocky surfaces above the sediment-water interface. The overall appearance and evidence of rapid formation suggest these crusts formed from a gel in sea water.

RÉSUMÉ

Des concrétions d'oxyde de manganèse et de fer sont actuellement en formation sur une crête sous-marine (filon-couche Patrick) dans la partie supérieure de l'inlet Jervis. L'auteur étudie la sédimentologie et l'océanographie du filon-couche Patrick et des bassins avoisinants afin de définir le milieu de la déposition.

Les sédiments du bassin supérieur proviennent principalement de la rivière qui se jette au fond de l'inlet. La grosseur moyenne des grains des sédiments superficiels, diminue uniformément à partir de la source. La répartition des sédiments dans le bassin inférieur diffère de façon marquée de celle que l'on a relevée dans le bassin supérieur en ce qu'il n'y a pas de source dominante de matériel mais plutôt plusieurs sources locales.

Les vestiges abondants de faune marine de hauts fonds trouvés dans des échantillons de sédiments qui reposent en eaux profondes indiquent que les sédiments déposés sous forme de deltas à l'embouchure des rivières et des ruisseaux glissent périodiquement au fond du bassin. La meilleur

explication des données sur la turbidité sédimentologique et optique du bassin supérieur serait le phénomène de glissement à partir du delta au fond de l'inlet accompagné de courants de turbidité ou de densité. Le filon-couche Patrick semble créer une barrière en aval de cet écoulement.

La minéralogie des sédiments de fond indiquent une source granitique. Le cartographie de la partie supérieure de l'inlet Jervis montre que ce dernier repose à l'intérieur d'un lambeau témoin de roches pré-batholitiques, surtout des argilites. Ainsi, les sédiments qui sont actuellement déposés sont des matériaux glaciaires remaniés provenant originalement de l'autre côté de la ligne de partage des eaux actuelle.

Les données recueillies semblent identiquer que le filon-couche Patrick est formé de roche en place recouverte de matériel glaciaire du Pléistocène. Le taux d'accumulation des sédiments récents sur le filon-couche est faible, surtout dans la dépression médiane. Les concrétions d'oxyde de manganèse et de fer, les croûtes d'oxyde de fer et les granules de glauconite et de montmorillonite ne sont en formation que dans cette dépression. On croit que les concrétions se forment par la précipitation d'oxydes de manganèse et de fer sur les cailloux et les galets qui reposent à l'interface sédiment-eau. Les ions métalliques sont mobiles dans le milieu réducteur des sédiments argileux-sableux sous-jacents mais se précipitent au contact du milieu oxygénant des sédiments superficiels. Les croûtes de fer se forment sur de grandes surfaces rocheuses par-dessus l'interface sédiment-eau. L'apparence générale et les indices de formation rapide pourraient vérifier que ces croûtes se sont formées à partir d'un gel dans l'eau de mer.

SEDIMENTATION AND MANGANESE CONCRETIONS IN A BRITISH COLUMBIA FIORD (JERVIS INLET)

INTRODUCTION

History and Purpose of the Study

A sedimentologic survey of Jervis Inlet was initiated in May, 1966 to supplement information obtained from other British Columbia fiords (Murray and Ricker, in prep.; Gucleur and Gross, 1964). There were two principal objectives; (1) to understand some of the factors controlling sedimentation in a deep-silled, medium run-off, low oxygen content fiord, and (2) to establish criteria from Holocene sediments which may be useful in recognizing and interpreting similar deposits in the geological record. In the process of systematic sampling of upper Jervis Inlet, a localized deposit of manganese-iron concretions (nodules) was found on a submarine ridge (Patrick Sill). Thereupon, a more intensive study of Patrick Sill and adjacent basins of upper Jervis Inlet was conducted. An understanding of all oceanographic aspects of Jervis Inlet should lead to a better understanding of the origin of manganese concretions in shallow coastal waters.

Location and Physical Setting

Jervis Inlet is located in the northwesterly trending Pacific Range of the Coast Mountains. The mouth of the inlet lies about 46 nautical miles (85 km) west-northwest of Vancouver, British Columbia, on the eastern margin of the Strait of Georgia. The inlet is 48 nautical miles (89 km) long and the width averages 1.7 (3.2 km) and seldom exceeds 2.5 nautical miles (4.6 km). Access to the area is by boat or aircraft only.

The study area (Fig. 1) encompasses the northern or upper part of the inlet which is divided into two legs or "Reaches" by a right-angle change in strike of the axis. Queen's Reach is uppermost and has a northwesterly trend while Princess Royal Reach trends to the northeast (Fig. 2). Princess Louisa Inlet, which opens into Queen's Reach, was not included in this study. Patrick Sill lies perpendicular to the axis of Queen's Reach at the point where Queen's Reach turns into Princess Royal Reach (Fig. 2; Fig. 3, in pocket).

Jervis Inlet, a glacially modified Pliocene river valley (Peacock, 1935), was invaded by the sea with the waning of the Pleistocene ice sheet. The mountains surrounding the inlet rise 6,000 to 8,000 feet (1800 to 2200 m) above sea level. Steep mountain sides dip at angles averaging 30 to 35 degrees to the water's edge and disappear below sea level with no change of slope. Deep striations on rock surfaces, mountain sides too steep and polished to trap soil to support vegetation, and hanging valleys, all indicate extensive glaciation.

Original manuscript submitted: January 16, 1973
Final version approved for publication: April 15, 1973
Authors' address: Department of Geological Sciences and Institute of Oceanography
University of British Columbia

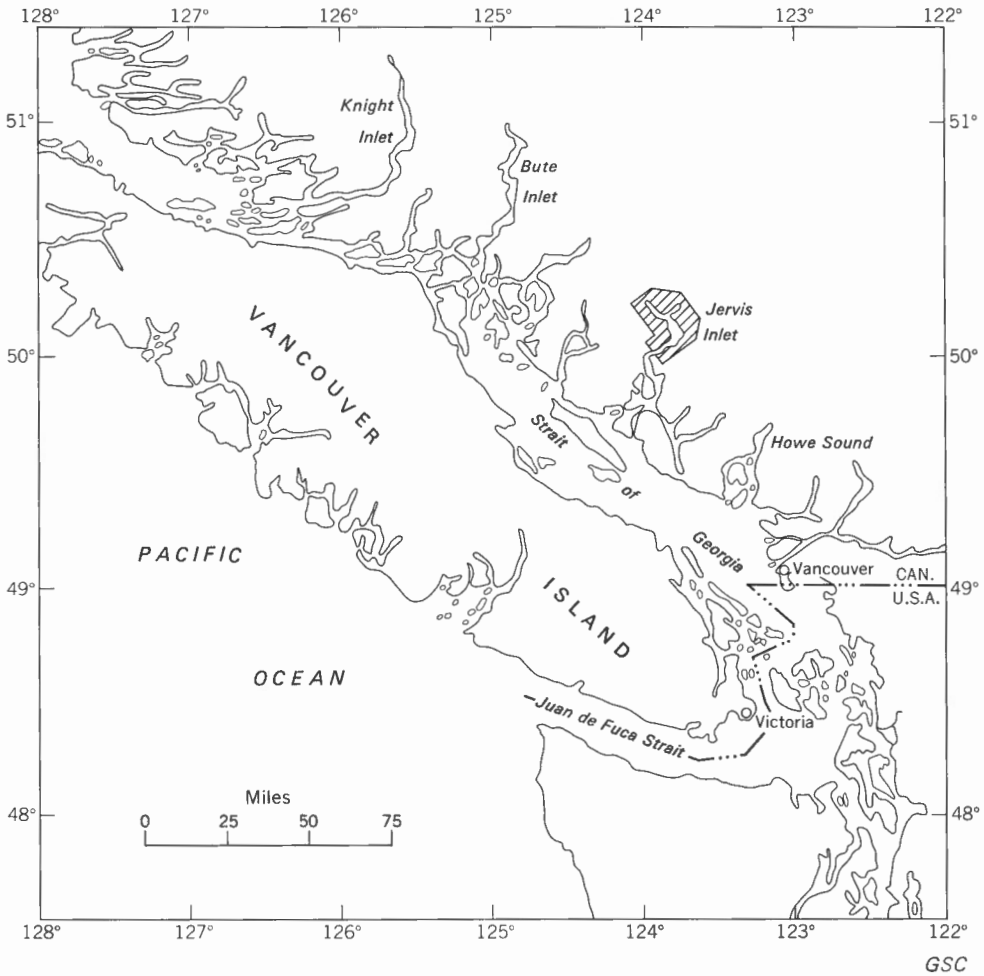

Figure 1. Index map.

The watershed area of upper Jervis Inlet is small, and many of the streams are intermittent. Queen's Reach and Princess Royal Reach have watershed areas of 273 and 167 square miles (855 and 523 km^2) respectively. Unlike the majority of long inlets, the run-off into Jervis follows the coastal rainfall pattern closely and is above average in the spring and winter months and below average during July through September. This is due to the absence of large, permanent snowfields within the watershed to store precipitation. The mean annual fresh water discharge into Jervis Inlet is 236 cubic yards (180 m^3) per second. In contrast, Howe Sound, which has a length of 23 nautical miles (42 km), receives a mean annual discharge of 630 cubic yards (480 m^3) per second (Trites, 1955). The average rainfall for southern inlets is estimated to be 60 to 100 inches (150 to 250 cm) annually at lower elevations (British Columbia Atlas of Resources, 1956). However, at higher elevations, the amount of precipitation can increase to 100 to 150 inches (250 to 380 cm) annually, especially towards the heads of the inlets. The inlets funnel moist Pacific air inland until, at the head, this air is forced to rise abruptly. About 10 to 15 per cent of precipitation falls as snow.

Previous Work

Prior sedimentological work in Jervis Inlet has been done only on a reconnaissance basis as part of an overall study of the British Columbia coastline (Pickard, 1956), and the continental shelf (Cockbain, 1963). More detailed sedimentological studies have been made in Bute Inlet (Toombs, 1956), Saanich Inlet (Gucleur and Gross, 1964) and Howe Sound (Murray and Ricker, in prep.).

The surficial geology of the upper Jervis Inlet area was mapped on a reconnaissance basis by LeRoy (1908). Since then no further work has been published for this area. Bacon (1957) described the bedrock geology of the Lower Jervis Inlet area. The Geological Survey of Canada is presently mapping the Jervis Inlet area.

The principal physical oceanographic features of Jervis Inlet have been studied by Pickard (1961). Detailed studies have been made on optical turbidity by Pickard and Giovando (1960) and on circulation by Lazier (1963).

Field Work and Acknowledgments

This work was financed by a contract between the Geological Survey of Canada and the University of British Columbia and formed the basis of a M.A.Sc. thesis by the senior author (Macdonald, 1970). Field work was carried out from the vessels C.S.S. Ehkoli and C.S.S. Vector of the Department of Energy, Mines and Resources. The assistance of the officers and crew of these vessels was invaluable. Detailed bathymetric charts (field sheets) of the study area were generously supplied by the Canadian Hydrographic Service.

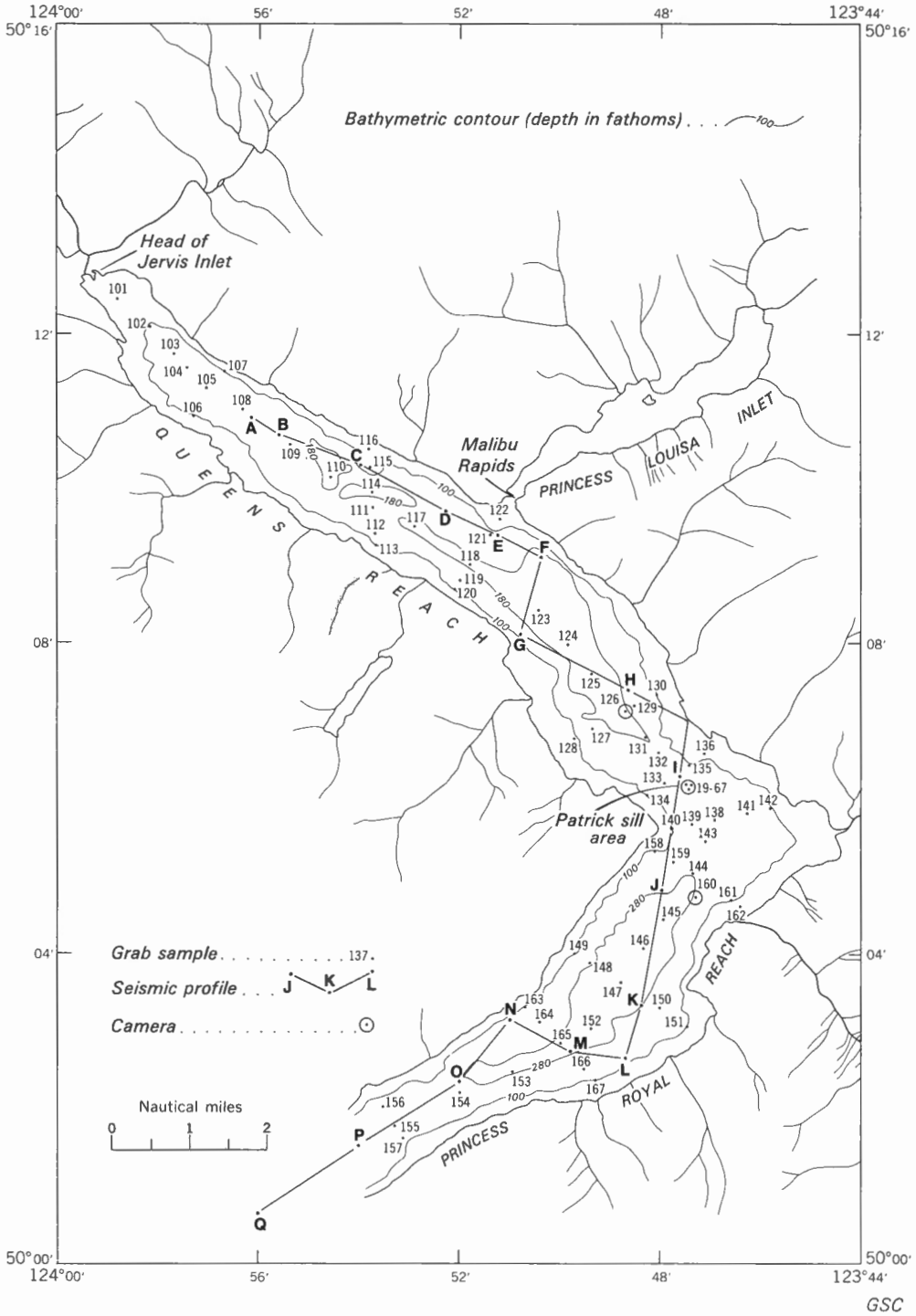

Figure 2. Sample station locations of Jervis Inlet (Northern portion).

Geomorphology of Southwestern British Columbia

Early Ordovician time may have marked the beginning of a series of tectonic events which ultimately formed the Insular and Coast Mountains region (Roddick, 1965).

Intense folding, metamorphism and uplift were accompanied by volcanism and the development of large plutonic masses. Successive stages of tectonism followed by erosion removed much of the rock cover from the batholithic cores. The derived sediments were deposited in flanking basins under marine and brackish conditions (Holland, 1964). The resulting land surface was a peneplain of low relief and average elevation of 900 to 1,200 feet (270 to 370 m) below the present average (Holland, op. cit.). Differential uplift of this erosion surface occurred during early Tertiary with greatest movement along two main axes of intrusion (Holland, op. cit.). Separating these axes, which are the present day Insular and Coast Mountains, was a trough now corresponding to the Strait of Georgia. Sediments derived from further erosion of rejuvenated areas were deposited in this coastal trough along with lavas and fragmental products of regional volcanism. Erosion continued through the middle Pliocene and further unroofed the granitic cores of the uplifted areas. The land surface was reduced to low or moderate relief of 1,500 to 2,000 feet (460 to 610 m) (Holland, 1964). Late Pliocene time marked the advent of renewed differential uplift along the previously active axes resulting in rejuvenation of the erosive power of all the streams. The late Tertiary erosion surface was deeply dissected and partially, to almost completely, destroyed. The present topography is essentially that of the late Pliocene, considerably modified by Pleistocene glaciation.

During Pleistocene time, southwestern British Columbia was extensively glaciated by cirque, valley, and continental glaciers (Armstrong, et al., 1965). Studies indicate at least two major Cordilleran ice sheet glaciations separated by an interglacial stage. Peripheral areas may have been subject to three or more major ice advances. The sequence of major Pleistocene events is shown in Table 1 (Appendix A).

The valley glaciers widened and deepened trunk valleys to a U-shaped cross-section leaving truncated spurs, hanging valleys and scoured rock surfaces. A result, perhaps not immediately evident, was the over-deepening of many of the valleys. For example, the maximum depth in Jervis Inlet, 385 fathoms (705 m), occurs about 10 nautical miles (18 km) from the mouth. This depth exceeds by 178 fathoms (326 m), the maximum depth in the Strait of Georgia. The valley glaciers that flowed into the Strait of Georgia coalesced and moved south and southeast down the Strait.

The ice sheet that accumulated during the Vashon stade attained an estimated thickness of from 5,000 to 8,000 feet (1500 to 2400 m). The weight of the ice sheet depressed the land surface with respect to sea level. The net effect of the waning of the ice sheet was the emergence of the land surface. The height of emergence, as measured from raised beach deposits near the mouth of Jervis Inlet was 424 feet (129 m), and 500 feet (152 m) at Campbell River (Holland, 1964). With the retreat of the Cordilleran ice sheet, the heavily scoured and probably nearly sediment-free inlets became depositional basins for glacial and glaciomarine sediments.

The structural pattern of the British Columbia coastline, resolves into two two-component systems. The dominant system consists of elements arranged northwest – southeast and northeast – southwest, i.e. longitudinal and transverse to the trend of the coastline. A subordinate pattern is oriented north-south and east-west (Peacock, 1935).

Most of the inlets have abrupt, high angle changes in the strike of their axes, a feature explainable by structurally controlled fluvial erosion. Rejuvenation of the earlier Pliocene erosion surface during the late Pliocene (Peacock, 1935) created a deeply dissected and immature topography before Pleistocene glaciations. Thus, fiords are believed to be the drowned lower parts of immature valleys developed by fluvial erosion and modified by intense glacial action (Peacock, 1935).

Two dominant characteristics of British Columbia and Norwegian fiords are extensive over-deepening and general presence of one or more thresholds, or sills, along their length (Pickard, 1956; Strøm, 1936). Over-deepening is apparently related to glacial erosion but the origin of the sills is debatable. Some sills are resistant granitic rock which for part of their length rise above sea level as islands or extend the shoreline to create a narrows. Other sills, are thought to represent terminal moraines deposited at points of farthest advance of valley glaciers.

METHODS OF STUDY

Sample localities (Fig. 2) were selected in order to obtain bottom material from all representative environments in upper Jervis Inlet. Positions were ascertained by combined use of echo sounder, Decca radar and/or sextant. Surficial sediments were obtained using a 1/6 square metre Pettersson grab sampler. Cores of bottom sediment were obtained by using a 1 1/4-inch-diameter Phleger corer and a 2 3/8-inch-diameter gravity corer. Underwater photographs were obtained by an Edgerton, Germeshausen and Grier photographic assembly.

Bathymetric maps (Fig. 3, in pocket, and Fig. 18) were prepared from Field Sheet No: 2228-L of the Canadian Hydrographic Service and echo-sounding surveys completed over Patrick Sill with a 38 KHz Kelvin-Hughes sounder. A continuous seismic profile from the head to the mouth of Jervis Inlet (Tiffin and Murray, 1966) was obtained using a 5000-joule Edgerton, Germeshauen and Grier sparker system, hydrophones, a Geospace amplifier and an Alden Precision Graphic Recorder.

Grain size analyses were made by dry sieving and hydrometer (Fig. B-1, Appendix B; Macdonald, 1970). Mineral analyses of the sand sized fraction were carried out on select samples by point counting. Clay minerals were separated into the different size fractions (Kittrick and Hope, 1963) and X-ray diffraction analyses were conducted on fractions using standard chemical and heat treatments (Macdonald, 1970). Carbon analyses were made using a Leco induction furnace and CO_2 absorption system. Polished sections of manganese concretions were examined under reflected light.

PHYSICAL OCEANOGRAPHY

Jervis Inlet has been grouped by Pickard (1961) with those inlets that receive medium run-off with little or no contribution from glaciers or permanent snowfields. Studies by Lazier (1963) revealed that the average salinity-depth profile showed a lack of a homogenous surface layer of low salinity and no distinct holocline. Surface salinity reached 50 per cent of deep water salinity in about one fathom and 90 per cent of the deep water salinity within a depth of 4 to 11 fathoms (Pickard, 1961). The average temperature-depth profiles resemble the salinity-depth profiles (Lazier, op. cit.).

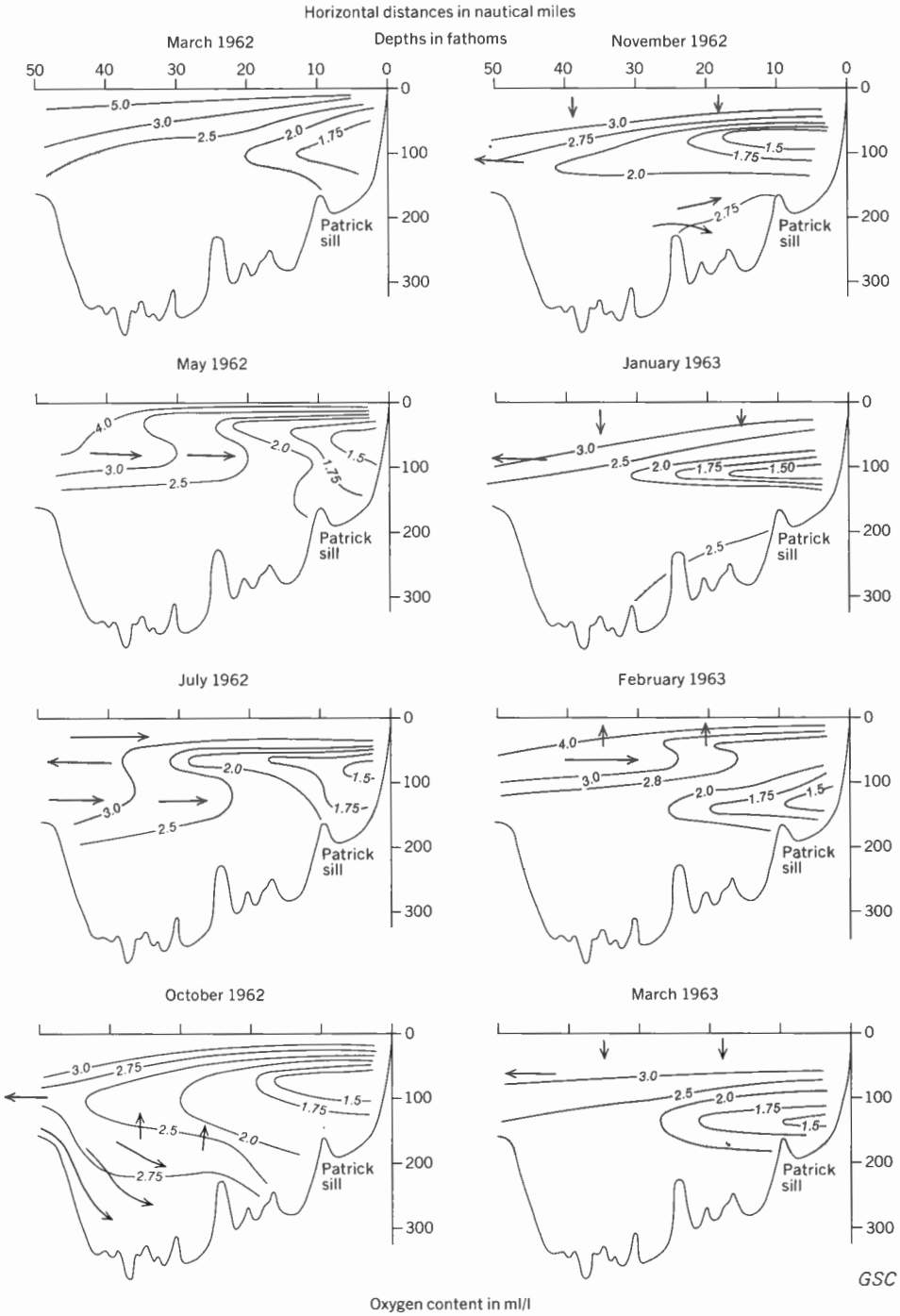

Figure 4. Water circulation as indicated by longitudinal oxygen profiles after Lazier, 1963 (see Figure 3 for line of section).

Jervis Inlet is classed as a deep-silled inlet as the sill at the mouth is deep enough to allow tidal waters to enter and leave without unduly modifying the vertical stratification of the resident inlet waters. Since the surface run-off into Jervis Inlet is small, the estuarine circulation (characterized by the lower salinity surface layer flowing seaward) is generally weak. Oxygen content-depth profiles (Fig. 4) are characterized by a mid-depth oxygen minima near the head of Jervis Inlet where the oxygen content of the water decreases to 1.5 millilitres per litre. This mid-depth oxygen minima is attributed to slow removal of water near the head of the inlet due to weak estuarine circulation.

The mean tidal range in Jervis Inlet is 11.1 feet whereas the largest tide reaches 17.1 feet (Canadian Tide and Current Tables, 1969). The time of either high or low water at the head of the inlet is not more than ten minutes later than at the mouth. Further, the tidal range at the head is 1 to 10 per cent greater than at the mouth (Pickard, 1961).

Pickard and Giovando (1960) studied the optical turbidity of surface and subsurface waters. They found the largest turbidity values at the head of the inlet in the low-salinity surface layer, uniformly lower values in the main water mass and then an increase in the optical turbidity at depth toward the head of the inlet above Patrick Sill. The increase in turbidity may be due either to tidal currents (Pickard and Rodgers, 1959) scouring the bottom or alternately to turbidity currents originating at the head of the inlet (Pickard, 1961).

BATHYMETRY, BASIN STRUCTURE AND SEDIMENT THICKNESS

The study area encompasses two basins (Fig. 3, in pocket) separated by a sill (submarine ridge). The upper or more northerly basin coincides with Queen's Reach, while the lower coincides with the upper two-thirds of Princess Royal Reach.

The sill depth of the upper basin is 160 fathoms (290 m) and that of the lower is 220 fathoms (400 m). The maximum depths are 190 and 290 fathoms (348 and 530 m) respectively. The bottom slope along the basin axis at the head of the inlet measures 1°50', but rapidly increases to 10°36' and then decreases to 0°14' (average) for most of the length of the upper basin. The slope of the bottom of the second basin is approximately 0°02'. The south-facing flank of Patrick Sill dips at 18°30' on the axial line but the angle increases towards the inlet sides.

Transverse sections (Fig. 5) illustrate the modified catenary or U-shaped cross-section which is typical of glacially scoured valleys. In the upper basin, the 160-fathom (293 m) contour marks the approximate break in slope between the sides and bottom of the inlet. In the lower basin, the break in slope occurs at 280 fathoms (513 m). The slope of the inlet sides ranges from 10 to 47 degrees and probably averages about 35 degrees. Pickard (1961) noted from transverse sections that a flat bottom was characteristic of the upper basin and was most pronounced just inside the sill at the deepest portion of the basin. This plus optical turbidity data led him to postulate the existence of turbidity currents within the upper basin.

Information of sediment thickness and basin structure can be obtained from Figure 6, a line-drawn interpretation of a continuous seismic sparker profile. Many of the apparent peaks on the record result from the zig-zag course of the ship (see insert, Fig. 6) and hence they reflect the ship approaching and then turning away from the shoreline.

Estimates were made of the total Quaternary (Recent and Pleistocene) sediment thickness in the different basins, assuming the average speed of sound in soft sediment to be 7,000 feet per second (Dobrin, 1960, gives Vp = 4,800 to 7,800 feet/second in Recent and Pleistocene sediments). In the upper basin, the average sediment thickness is in the range of 450 to 500 feet (150 - 165 m). The thickness increase in sections F - G reflects lateral addition of sediment from the adjoining Princess Louisa Inlet. In the lower basin, the average sediment thickness increases to 700 feet (230 m). Determination from seismic records of sediment thickness on steep slopes such as the inlet walls and the sill is difficult due to the omni-directional nature of the transducer. However, the action of the grab sampler indicated sediment cover is thin to lacking in these areas. Over the sill, photographs suggest, but do not prove, the presence of bedrock.

Sills near the upper ends of inlets have often been explained as terminal moraines marking the point of farthest advance of Sumas stade glaciers. The concavo-convex bathymetry of some sills such as the inner sill of Howe Sound tend to support this idea. However, recent seismic records (1972) indicate bedrock control even in this case. Many sills are located at points where feeder glaciers met trunk glaciers (e.g. Malibu Rapids) or at points where the valley of the trunk glacier widened (e.g. inner sill of Howe Sound) or abruptly changed strike (e.g. Patrick Sill). The dynamics of ice flow and wasting under these circumstances may be important considerations in explaining the location and shape of sills.

SEDIMENTS

The surficial sediments were classified texturally according to Shepard (1954). Basically, the sediments consist of equal parts of silt and clay-sized particles (Fig. B-2, Appendix B) with variable amounts of sand and gravel (0.5 to 85%). Similar characteristics are presented by Cockbain (1963) for Vancouver Island inlets, but his data for mainland inlets, plotted in the same manner, indicate a slight skewness toward clay-sized particles, with the average abundance of sand and gravel less than for Jervis Inlet.

Sediment grain size distribution (Fig. 7) along the axis of upper Jervis Inlet is presented as a reference for the discussion on total carbon content, free iron content and mineralogy of the sediments. In each of the figures similar to Figure 7 the data being presented are superimposed on the bottom profile taken along the inlet axis.

Colour

The colour of the wet sediments is characteristic of the coastal marine province varying from a greyish olive (10Y4/2) to an olive grey (5Y3/2). The sediments of the upper basin are more lightly coloured (i.e., greyish olive) whereas those in the lower basin are a darker olive grey colour. Samples collected along the axes of the lower basin from Station J-146 southward contained varve-like laminations of olive-grey alternating with black coloured sediment which contained distinct concentrations of H_2S. In the upper basin, samples containing noticeable concentrations of H_2S were collected nearshore in relatively shallow waters (Stations J-101, J-102 and J-128).

Cores (E.V. Grill, oral comm.) indicate the presence of a thin (0.5 to 1.5 cm), very fluid, dark yellow-brown to red-brown oxidized layer at the sediment-water interface over most of the area. This oxidized layer was only observed in grab samples from the manganese concretion locality where it thickens to several centimetres and includes a layer of coarse sand to cobble-sized sediment.

The olive-green colour of the wet sediments is due primarily to the organic content (Pantin, 1969). Reduced iron may add to the overall colour effect. However, a closer apparent correlation exists between total carbon content and the darker coloured sediment of the lower basin than with the extractable iron content (compare Fig. 8 with Fig. 9). When air dried at room temperature, the sample colour becomes light grey to light green-grey.

Total Carbon Content

The total carbon content (Fig. B-3, Appendix B) was determined for each of the surficial samples collected. Figure 8 shows the carbon content in comparison with the weight per cent of clay size particles along a longitudinal profile. The total carbon percentage can be converted to an organic matter percentage by a 1.8 multiplication factor (Trask, 1938).

In general, the trend in the total carbon content of the sediment shows a gradual increase with distance from the head of the inlet. This trend is interrupted in the area of the "V"-notch of Patrick Sill which presumably represents a much higher energy environment than its surroundings. In detail, Figure B-3 (Appendix B) illustrates the difference in total carbon distribution between the upper and lower basins. Most noticeable is the relatively constant distribution in the upper basin versus the zonal distribution in the lower basin. The total carbon content of the upper basin is in the 2-3 per cent range with the exception of certain nearshore areas and the slope at the head. Dilution and possibly lower productivity account for the low values at the head whereas the localized, nearshore areas of higher carbon content coincide closely with log-booming grounds or streams draining logged areas. The lower basin can be divided into three apparently distinct zones on the basis of carbon content. The nearshore zone has a low carbon content (<2%) and is coextensive with the steep walls. The intermediate zone, with an average carbon content of 2-3 per cent, coincides with the break in slope between the walls and floor, while the deep zone, with a carbon content of 3-4 per cent coincides with the basin floor.

Free Iron Content

Free iron was extracted from samples in preparation for X-ray diffraction analysis by a process of treatment with hydrogen peroxide (H_2O_2) and sodium dithionite (Macdonald, 1970). The extractions were then analyzed for iron by atomic absorption and the results (Fig. 9) are the sum of the irons extracted by the two methods.

The concentration of the iron extracted by sodium dithionite is relatively constant with distance from the head of the inlet, averaging about 0.39 per cent (3500 ppm). The state of this iron in the sediments is probably as poorly crystalline particulate iron oxides and as iron adsorbed to clay

minerals. A ratio of iron extracted by sodium dithionite to percentage of clay-size particles (all the samples had the same initial weight) indicates a decreasing trend from the head of the inlet. E.V. Grill (oral comm.) studied the metal content of sea waters from upper Jervis Inlet and showed the source of particulate iron to be the river at the head. Isopleths of suspended iron oxide content are approximately vertical with decreasing gradient from the source. Since the ratio curve tends to approach a base level, the curve shape may indicate dilution of particulate iron with distance from the source, while iron adsorbed by clay-size particles (of which approximately 70 per cent are clay minerals and micas) remains constant.

The chemical state of the iron within the sediment extracted by hydrogen peroxide is unknown. Possibly it is associated with the organic material since a correlation exists between iron extracted by peroxide and total carbon content.

The area with sediments containing minimal extractable iron corresponds to the manganese-iron concretion locality on Patrick Sill. The total carbon content and the percentage of clay-sized particles is also at a minimum because of the higher energy of the environment. Iron crusts recovered from the locality indicate precipitation from sea water on exposed rock surfaces.

Particle Morphology

Mineral grains from the 500-300 /μ (1.0-1.5Ø) and 88-63 μ (3.5-4Ø) fractions were examined by binocular microscope to determine the general shape and roundness and, if possible, any trends. Generally, the mineral grains were angular (Fig. 10a) indicating erosion by physical processes followed shortly by deposition with little or no reworking. Along the axis of the basins, however, subangular to subrounded grains were found at the inlet head and on the concretion locality (Fig. 10b). A transverse section, just above Princess Louisa Inlet indicated the central basin sediments to be better rounded than slope sediments but a similar section along the crest of the sill indicated the opposite in that angularity increased with depth. A third transverse section, across the lower basin, indicated more rounding with depth.

If rounding of mineral grains is occurring in situ, the areas with greatest current action are the head of the inlet and the concretion locality.

Mineralogy

1. Granule and larger size material (>2.0 cm)

Thin sections were cut from cobble-sized fragments of each of the major rock types present in the sediments. Rocks of approximately quartz diorite to quartz monzonitic composition accounted for 65-75 per cent of the granule-sized and larger material recovered in grab samples. Granite and minor pegmatites accounted for 5-15 per cent, volcanics (usually basaltic) for 5-20 per cent, and slates with occasional hornfels and amphibolite fragments for 0-5 per cent.

Hand specimens generally appeared fresh and revealed little evidence of alteration in the present marine environment, although some surface

alteration was apparent. Leucocratic rocks occasionally exhibited a light green to dark red-brown surface coloration. Polished sections show this stain to be a rind 1 to 5 mm thick. The red-brown stains may be due to absorbed iron oxides, whereas the green stains were possibly of organic origin.

In a typical quartz diorite cobble, sodic plagioclase (Ab_{60-70}) accounted for about 60 per cent of the rock. Quartz formed about 10 per cent of the rock and was usually anhedral and intergranular. Potassium feldspar occurred in minor quantities. Unlike plagioclase, these grains usually showed some signs of alteration. Also present were hornblende, sphene, zircon and magnetite. In some specimens, hornblende was the principal mafic mineral. In the more acidic quartz monzonite cobbles, quartz occupied about 45% of the section, K-feldspar 25%, plagioclase 25% and mafics and opaques 5%.

The average composition of the granites was 30-35% quartz, 55-60% K-feldspar and 5-10% plagioclase. The K-feldspar was often considerably altered.

The volcanic rocks were basaltic. A specimen of porphyritic basalt contained phenocrysts of plagioclase (An_{70}) and pyroxene with minor amounts of olivine, biotite, magnetite and hematite.

2. Sand size material (0.063-2.0 mm)

The mineralogy of fine sands (62μ to 125μ) was determined for 16 samples, collected along the inlet axis, by point counting thin-sectioned grain mounts. These fine sands contain the majority of the heavier mafic minerals and therefore, the calculated average composition will be skewed towards these minerals. The mineral percentages are given in Table 2 (in Appendix A) and an average composition of the fine sand fraction is as follows:

Plagioclase	37%	Biotite	5%
Quartz	24%	Epidote	3%
Amphibole	8%	Pyroxene	1%
K-feldspar	7%	Unidentifiable rock fragments and opaques	9%
Chlorite	6%		

There is a marked similarity of physical and optical properties of minerals between the fine sand fraction and the cobble fraction. Most of the coarse surficial sediments probably were derived from Coast Range batholithic rocks, as these are the only available source of granitic material. The average composition of granitic rocks (hornblende-quartz diorite) for the Coast Range Batholith south of Jervis Inlet calculated by Roddick (1965) is as follows:

Plagioclase	56%	K-feldspar	1%
Quartz	30%	Sericite	1%
Hornblende	7%	Opaques	0.5%
Biotite	5%	Chlorite	0.5%

Roddick's average composition does not correlate with the average composition of the fraction analyzed. This is predictable since the heavier minerals tend to be concentrated in the finer fractions.

The occurrence of minerals such as chlorite (6%), epidote (3%) and pyroxenes (1%) probably expresses the presence of pre-batholithic source rocks which are mapped as outcropping over most of the upper Jervis Inlet watershed (LeRoy, 1908).

Several trends were noted within the mineral groups (Fig. 11). Biotite, which gradually increases in abundance from the head of the inlet, was usually a dark green colour. However, over the sill, a red-brown variety predominates. Whether this effect is geochemical or an expression of past and/or present sedimentation patterns is not known. Hornblende was the only amphibole present from the head of the inlet to Station J-118. However, from J-118 to the end of the study area, tremolite-actinolite was also found, although never with the same abundance as hornblende.

Even though sediment is being added to the inlet elsewhere than at the head, the uniform sediment mineralogy from Station J-110 down the inlet indicates most of the sediment sources have the same mineralogy.

3. Clay size material

X-ray mineralogical analyses of clay sized particles were made on the same samples as those on which the mineralogy of the sand and cobbles had been determined. Interpretation of relative abundances of clays from diffractograms was made by comparison to three sample interpretations made by Dr. L.M. Lavkulich, Department of Soil Science, University of British

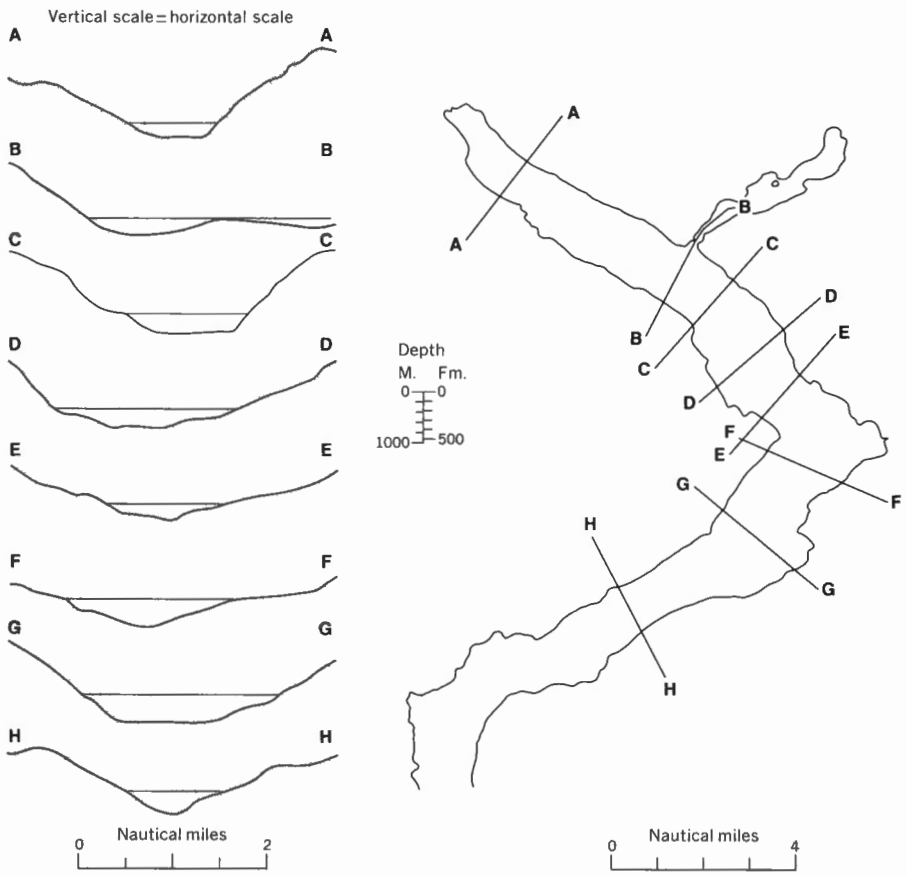

Figure 5. Transverse sections of Jervis Inlet (Northern portion). *GSC*

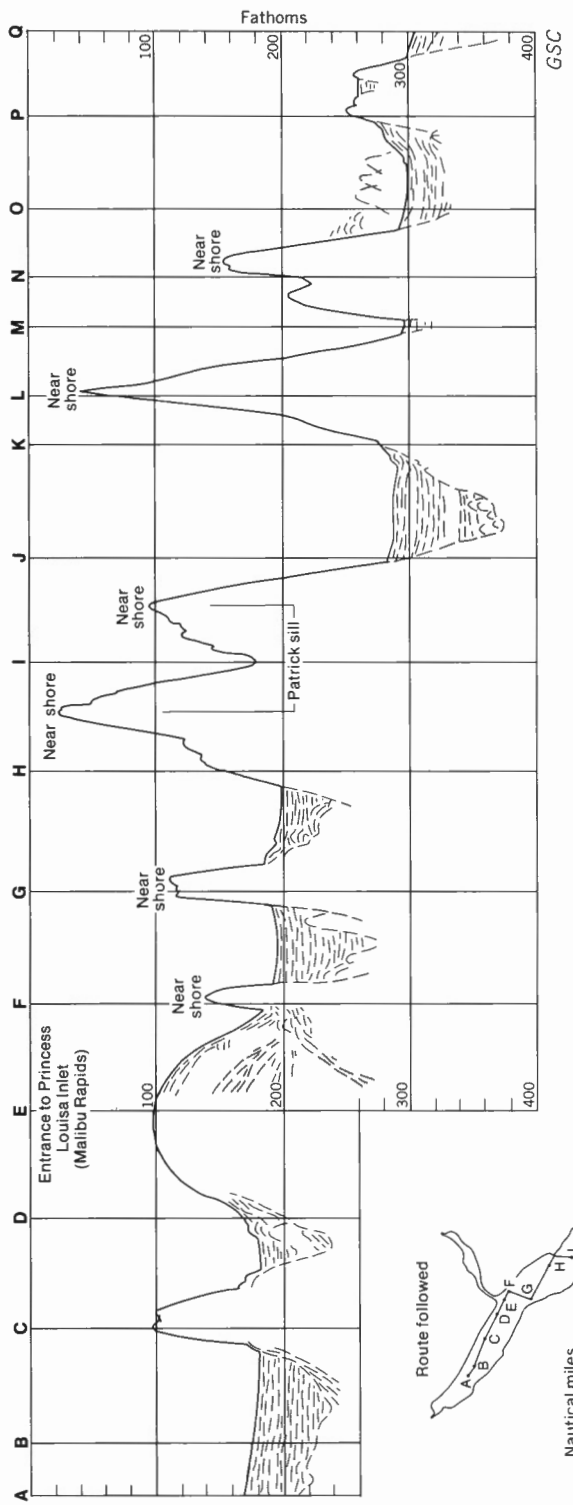

Figure 6. Line drawn interpretation of a continuous seismic profile along upper Jervis Inlet. Horizontal scale variable due to ships speed.

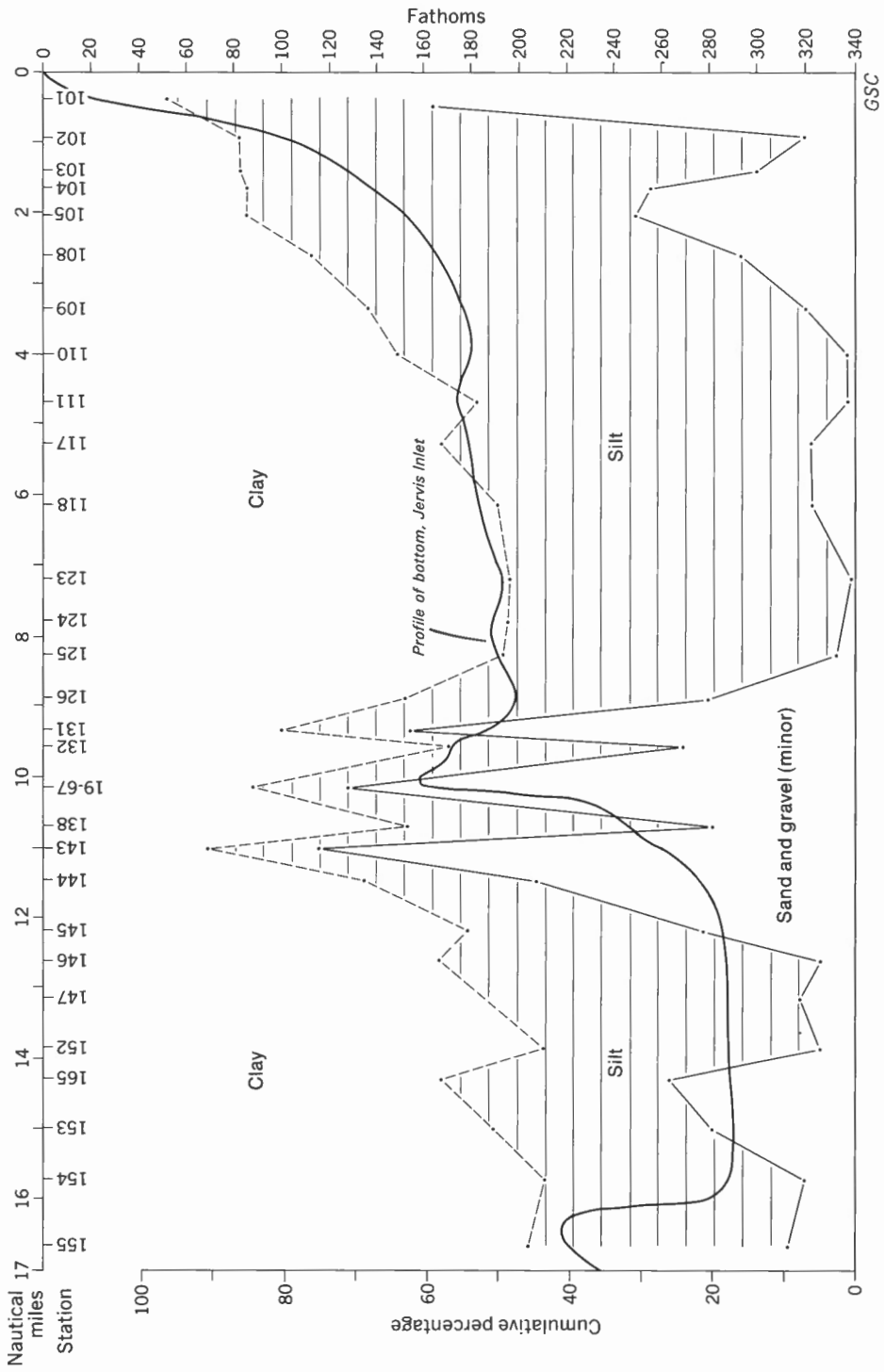

Figure 7. Grain size distribution along axis of upper Jervis Inlet.

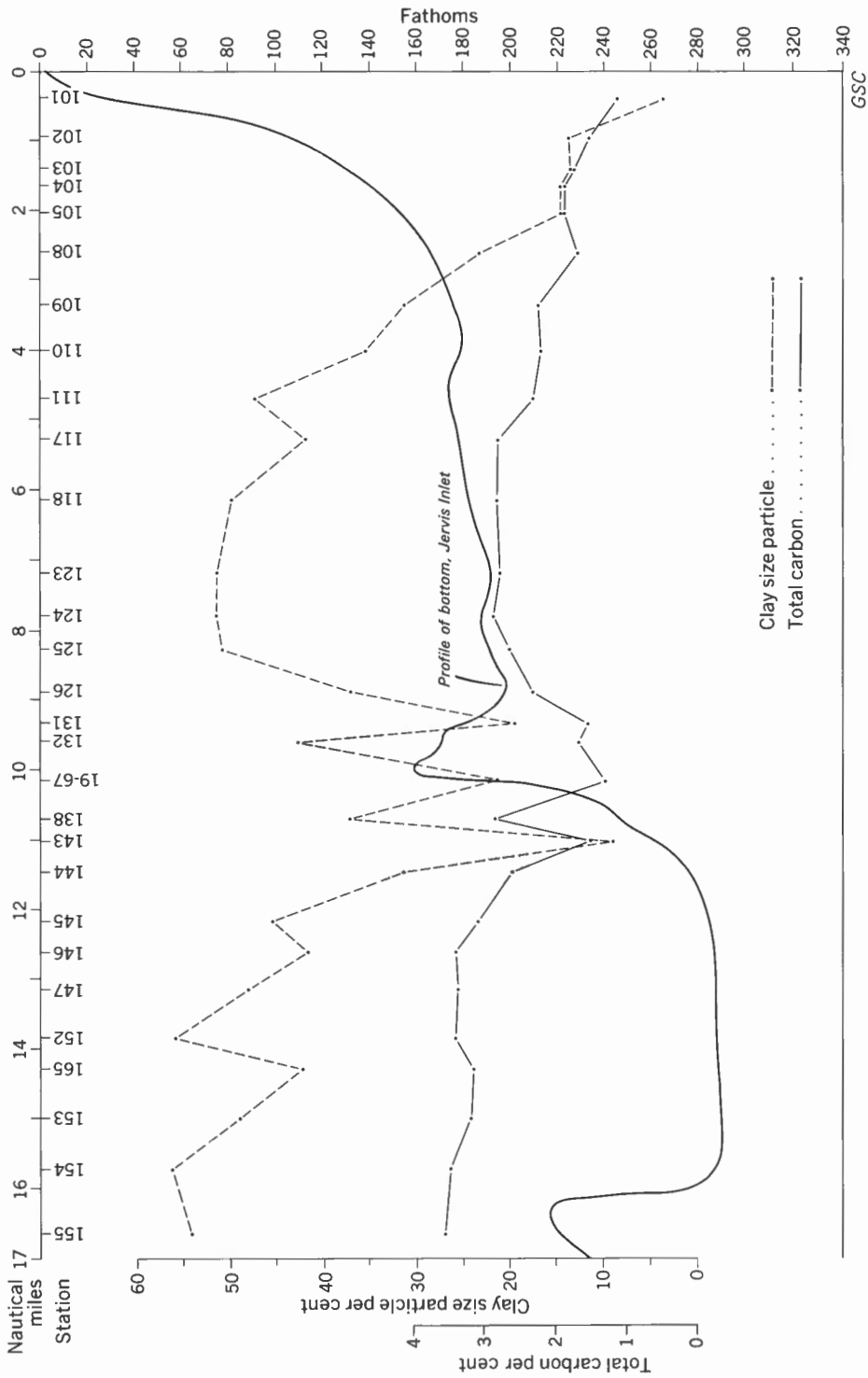

Figure 8. Clay size particule and total carbon content along axis of upper Jervis Inlet.

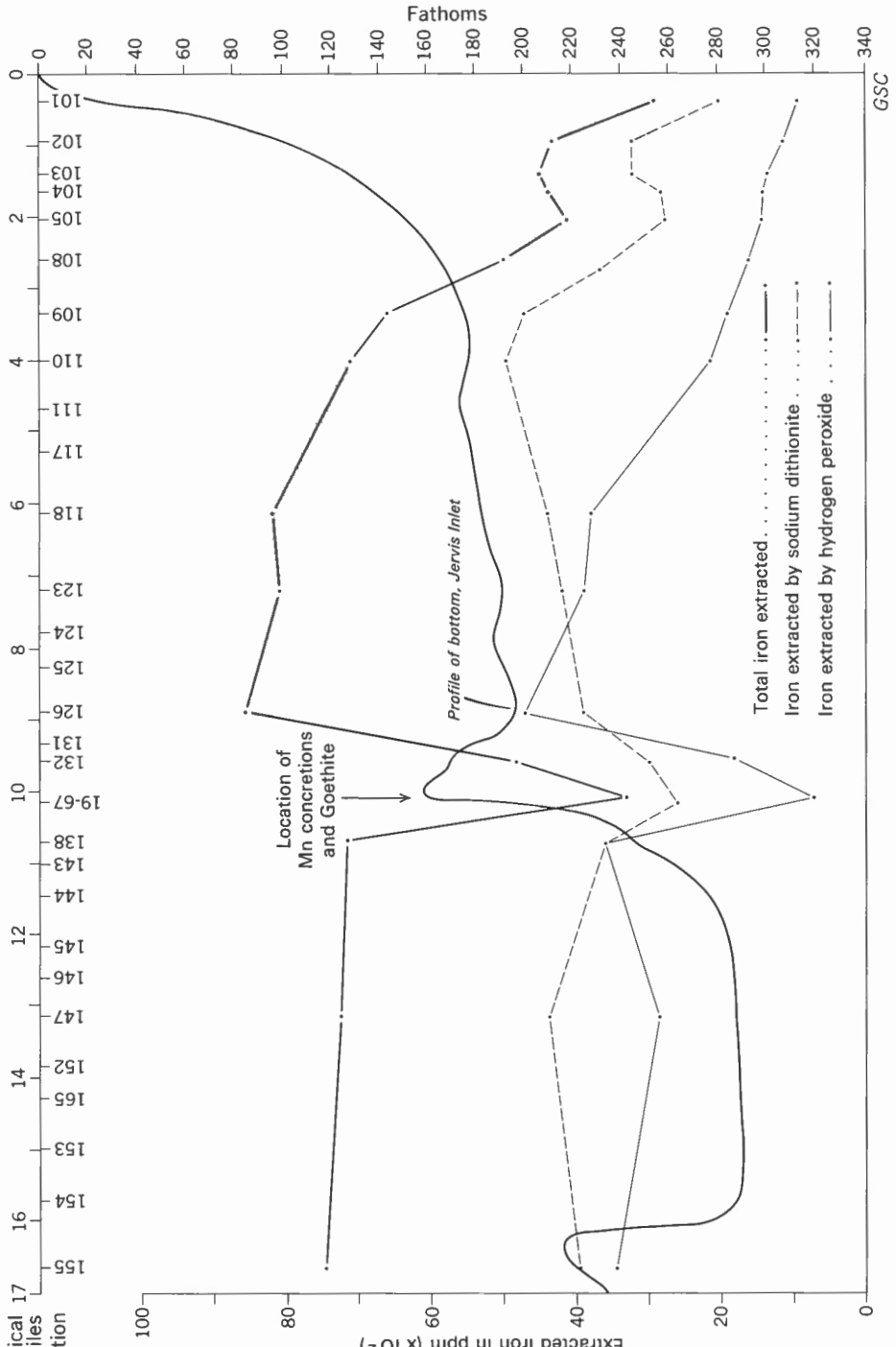

Figure 9. Iron extracted during sample preparation for X-ray analysis.

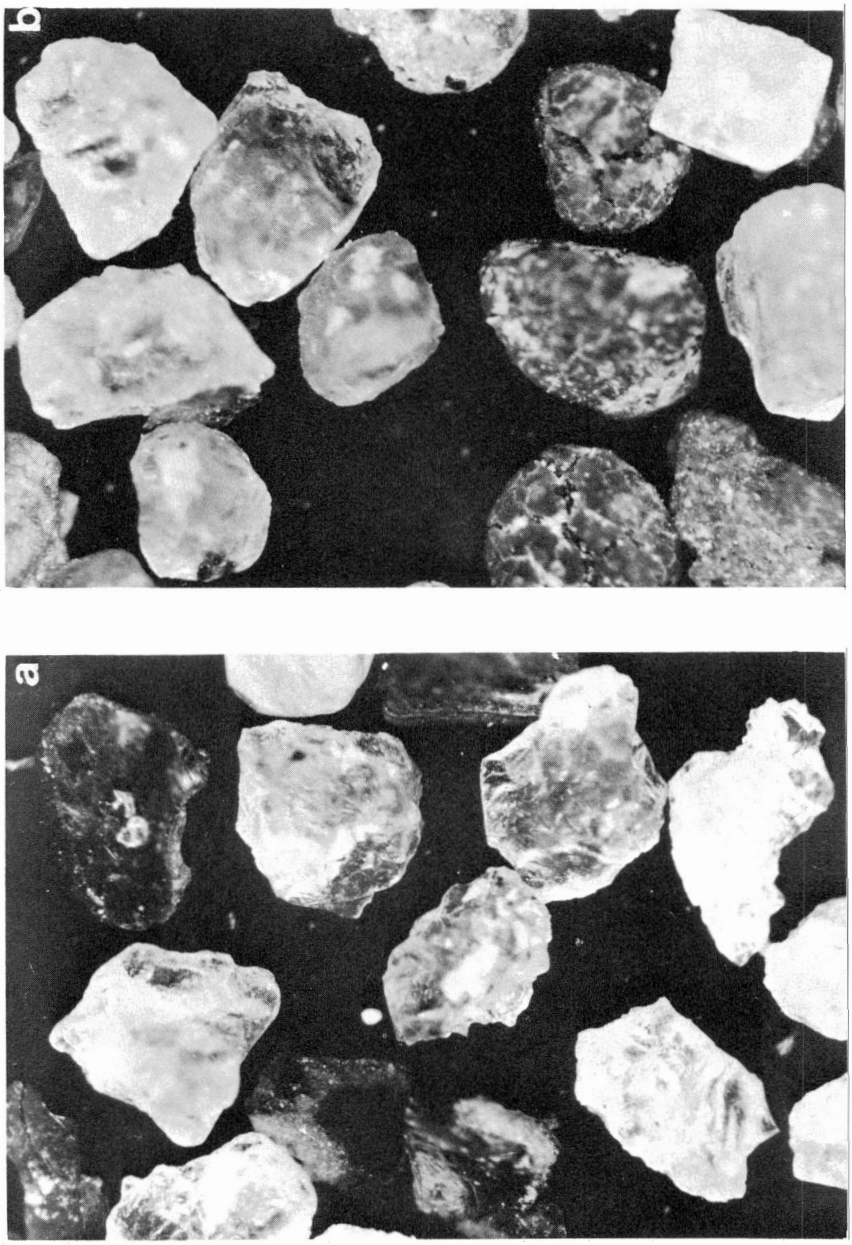

Figure 10

Columbia. The relative amounts of Fe, Mg and Al in the chlorites was based on diffraction patterns given by Weaver (1958). Table 3 (Appendix A) illustrates the clay and other mineral species present in the clay sized fraction and their 001 peaks (in angstroms) according to the heat and chemical treatment they were given.

Clay particle-sized rock flour is present (Table 4, Appendix A) as plagioclase feldspar, quartz and amphibole (principally hornblende) in nearly constant proportions for the length of the inlet, K-feldspar occurs as a trace mineral in considerably lesser quantities than plagioclase or quartz. However, off the entrance to Princess Louisa Inlet, K-feldspar content increases significantly.

There are several notable trends in clay mineral abundance in upper Jervis Inlet (Table 4, Appendix A). The most noticeable is the disappearance of montmorillonite and mixed-layer illite-montmorillonite by Station J-103, i.e. shortly after the material enters the marine environment. As these species disappear, vermiculite and mixed-layer illite-vermiculite appear. Illite-vermiculite occurs with an approximately constant abundance for the remaining length of the study area. Vermiculite gradually increases in abundance until, on the sill, it becomes the dominant clay mineral. For the remaining samples analyzed, vermiculite remains one of the dominant or near-dominant types. The overall trend is thus an increase in vermiculite with distance from the head of the inlet with the increase being accentuated on the sill. The only other trend noted was the appearance of mixed-layer illite-chlorite at Station J-109. This mixed-layer clay occurs in most samples taken farther down the inlet, but only in trace amounts. Illite and Fe and Fe-Mg chlorite have no noticeable trends in abundance.

Proponents of the differential settling of clay minerals to explain zonation (Grim, 1968) receive little support from the distribution data in Jervis Inlet. However, discrepancies may be due to scale. The rapid disappearance of montmorillonite and mixed-layer illite-montmorillonite with deposition in the saline environment suggest that potassium and magnesium are being absorbed from sea water by the montmorillonite. Absorption of these elements collapses the montmorillonite structure resulting in the formation of illite and chlorite.

Figure 10 (opposite). Photomicrographs of sand grains.

a) Station J-126 (approx. 60 x) Photomicrograph of mineral grains from medium sand fraction (350 to 500 μ). Note angularity and apparent concoidal fracturing of quartz grains. GSC Photo No. 202279-A.
b) Station J-19-67 (approx. 60 x) Photomicrograph of mineral grains from medium sand fraction (350 to 500 μ). Note rounded, partially dessicated pellets in lower half of photograph. These are tentatively identified as glauconite-montmorillonoid pellets. About 1/8 scale. GSC Photo No. 202279-B.

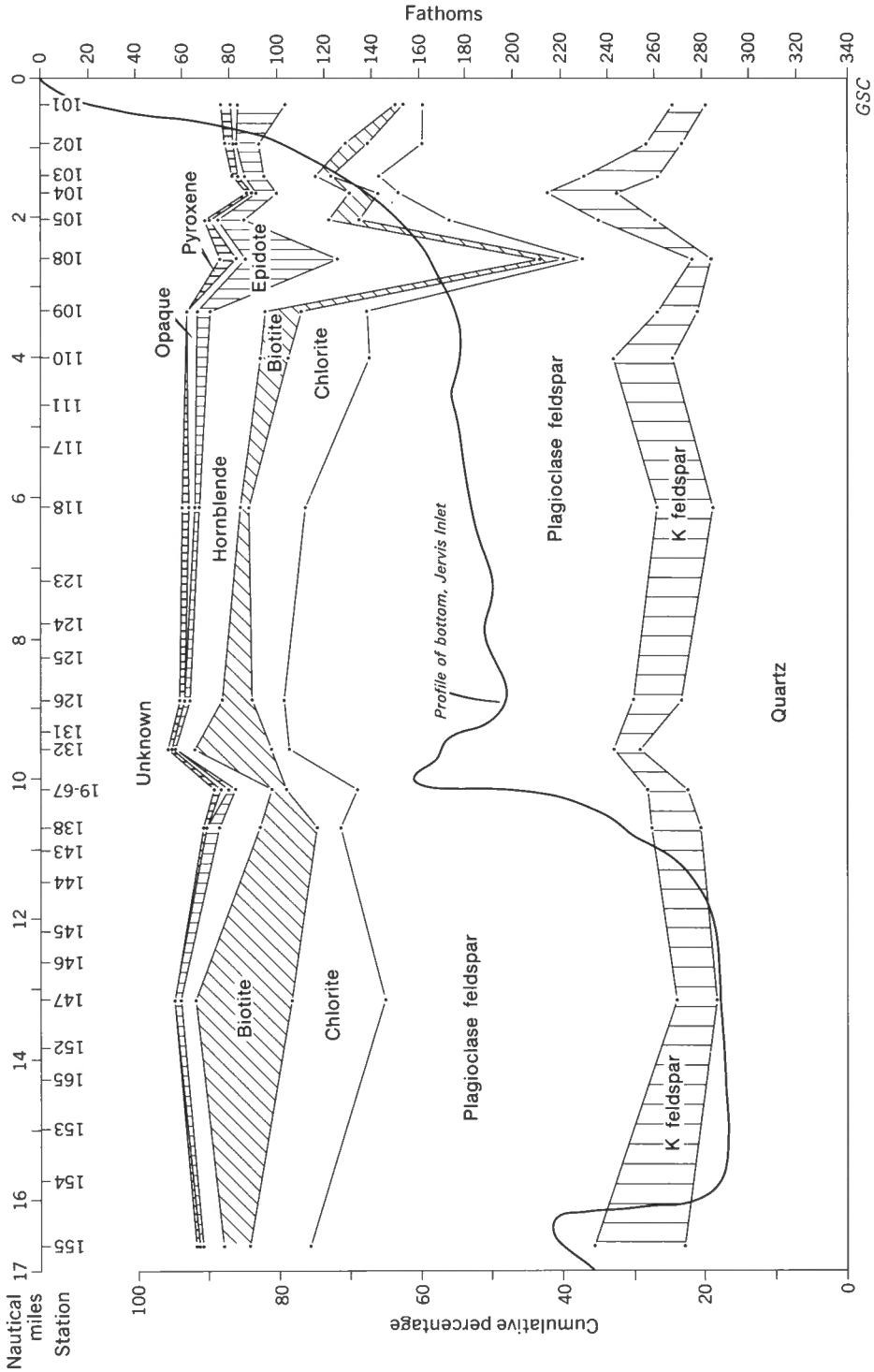

Figure 11. Mineral distribution along axis of upper Jervis Inlet.

Grain Size Distribution

The grain size distribution and corresponding sedimentary parameters were calculated with a computer program. Calculations were based on a cumulative curve plotted with arithmetic ordinates and developed by joining successive data points with straight lines. A minimum grain size was needed in the program and was arbitrarily set at 0.06μ (14Ø). Equations for sedimentary parameters (summarized by Folk, 1966) used in this interpretation were taken from Folk and Ward (1957) and are as follows:

Graphic Mean (Average particle diameter) = $M_z = \frac{Ø16 + Ø50 + Ø84}{3}$

Ø16, Ø50 and Ø84 are the Ø values taken from a cumulative curve for the appropriate percentiles

Inclusive Graphic Standard Deviation (Sorting of population)

$$= 0_1 = \frac{(Ø84-Ø16)}{4} - \frac{(Ø95-Ø5)}{6.6}$$

Skewness (Asymmetry of cumulative curve)

$$= S_{k1} = \frac{Ø84-Ø16+2Ø50}{2(Ø84-Ø16)} + \frac{Ø95-Ø5-2Ø50}{2(Ø95-Ø5)}$$

Kurtosis (Measure of peakedness of cumulative curve)

$$= K_G = \frac{Ø95-Ø5}{2.44(Ø75-Ø25)}$$

Since the Ø diameter is defined as $-\log_2$ (particle diameter in millimetres) a trend showing an increase in Ø value indicates a decrease in particle size.

The graphic mean which reflects the average particle diameter, gives no indication of the range of grain size diameters and for interpretive purposes the inclusive graphic standard deviation must be considered simultaneously. The skewness measures the degree of asymmetry and a negative value indicates a distribution curve asymmetric to the left (i.e. excess of coarse material), while a positive value indicates asymmetry to the right, (i.e. excess of fine material). A skewness value is a pure number and the absolute limits are -1.00 and +1.00. Kurtosis is a measure of peakedness of a curve, and is a ratio between sorting in the tails and sorting in the central position. Low values for kurtosis (i.e. 0.9) indicate better sorting in the tails than in the central portion. A distribution with low kurtosis is often bimodal. As with skewness, a kurtosis value is a pure number with limits of the measure being +0.41 and infinity with most samples falling in the 0.6 to 5.0 range (Folk, 1961).

Figure 12

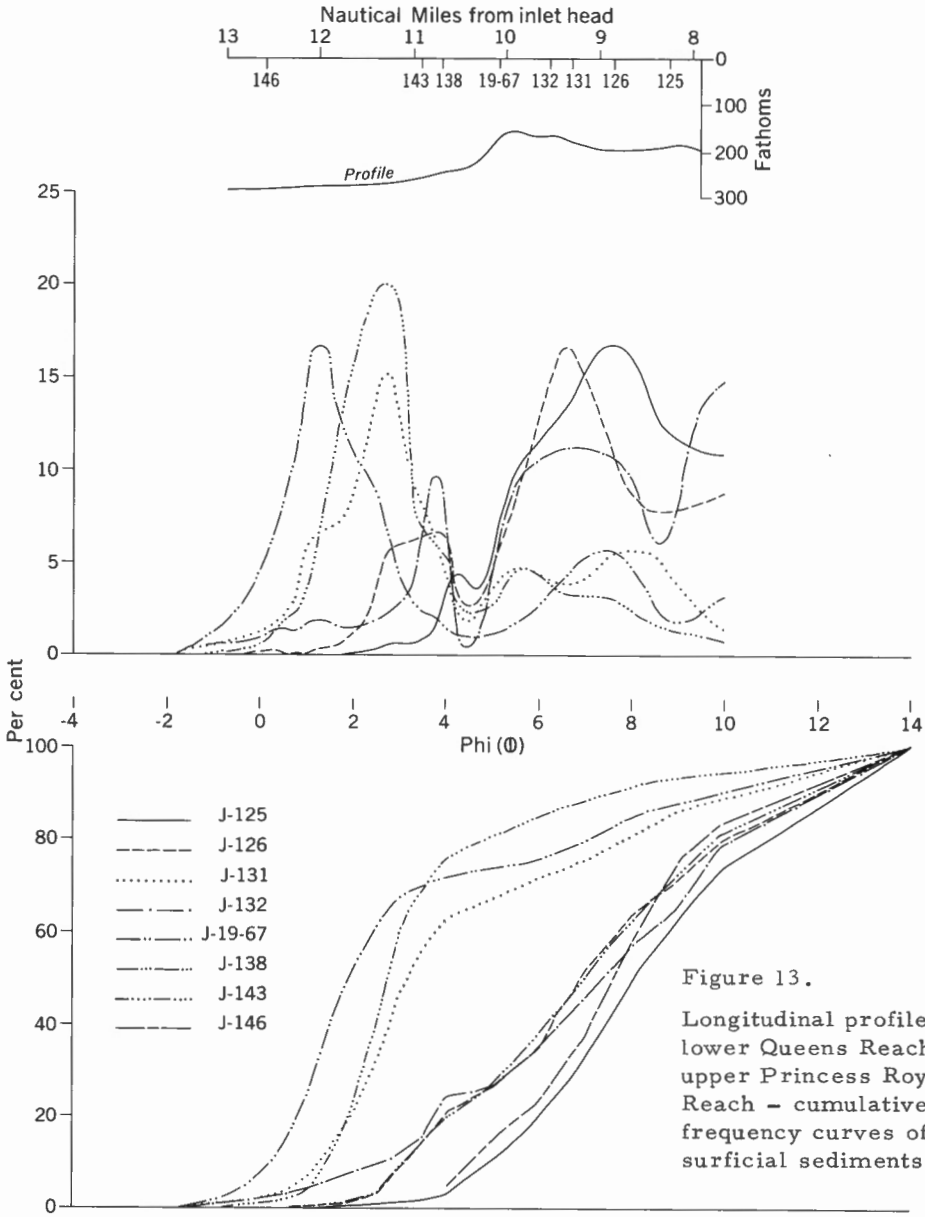

Figure 13.

Longitudinal profile of lower Queens Reach and upper Princess Royal Reach – cumulative and frequency curves of surficial sediments.

Figure 12 (opposite). Bottom Photograph – Station J-126. Note hummocky microtopography. This may be due to the presence of animals or to deposition processes (about 1/8 x). GSC Photo No. 202279.

The scale of the bottom photographs depends on the camera to sea floor distance. Where present, the compass assembly can be used as a scale indicator. The diameter of the compass dome is 3 inches (7.5 cm) and the length of the vane is 10 inches (25 cm). On an average, the photographs cover an area of about 3 feet by 4 feet (about 1 m x 1.3 m).

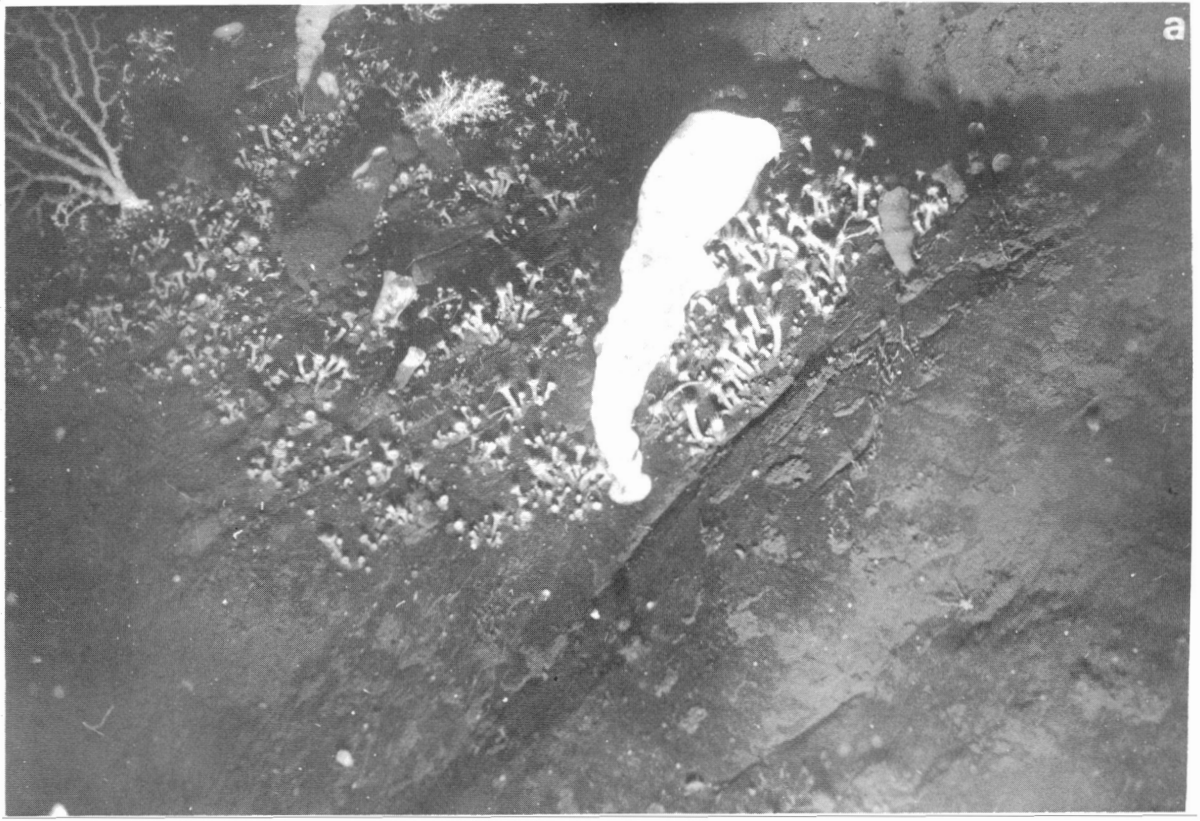

Figure 14a. Bedrock or large boulder in vicinity of concretion locality. Low rates of sediment deposition in this area allow animal growth. Plane of gorgonian coral in background is normal to current direction. (about 1/8 x). GSC Photo No. 202279-C.

b. Lag deposit in area of concretion locality. Note abundance of squat lobsters. (about 1/8 x). GSC Photo No. 202279-D.

Figure 14. Bottom Photographs – Station J-19-67.

Figure B-4 (Appendix B) shows the distribution of surficial sediments according to grain size in Jervis Inlet based on Shepard's (1954) classification. Similarly, Figure B-5 (Appendix B) shows the clay size particle distribution and Figures B-6 and B-7 (Appendix B) are longitudinal profiles of grain size distribution parameters.

Frequency curves plotted from the grain size analysis of the upper Jervis Inlet surficial sediments can be divided into two dominant modes. The coarse mode usually falls in the 250 to 63μ (2ϕ to 4ϕ) range, while the finer mode in the 16 to 4μ (6ϕ to 8ϕ) range. These ranges are the fine to very fine sands and medium silts to clays respectively.

Figures B-4 and B-8 (Appendix B) illustrate the uniform decrease in average particle diameter with distance from the head of the inlet within the upper basin. The particle size distribution of sample J-111 represents an approximate average for the upper basin (0.9% sand, 51.9% silt and 47.2% clay). For the sediment collecting on the floor of the upper basin, the graphic mean (in ϕ values) increases while the inclusive graphic standard deviation remains approximately constant. Overall, kurtosis follows a slowly decreasing trend and skewness an approximately constant trend. The principal source of sediment within the upper basin is therefore interpreted as the river delta at the inlet head. This source is, however, supplemented by an appreciable amount of material from Princess Louisa Inlet where ebb tides, with currents of up to 10 to 12 knots, deposit fine sand and silt (Figs. B-6 and B-7, Appendix B) in the deeper waters of Jervis Inlet.

Figure B-9 (Appendix B) presents the cumulative and frequency curves for a transverse section of Queen's Reach at a point above Malibu Rapids. The abundance of the coarse mode decreases with depth, while that of the finer mode increases.

Figure 12 is a bottom photograph taken at Station J-126 at a depth of 180 fathoms (330 m), the maximum depth in the upper basin. The photograph covers an area 3 by 4 feet (1 by 1.3 m). The microtopography appears hummocky. The origin of these hummocks is not known, but animals have some effect. However, photographs taken in an area where slumping is almost certainly occurring (Fig. 16) shows a similar topography.

Patrick Sill also shows interesting sedimentological features. The medial depression or "V"-notch and immediately adjacent areas are apparently areas of sediment reworking. Figure 13 illustrates how the sediment characteristics change in passing from the upper to the lower basin over Patrick Sill. The concretion locality (Station J-19-67) sediments have a mean diameter of 63μ (4ϕ) with a high standard deviation. Skewness is high and kurtosis low. A current is winnowing the sediment, leaving a lag deposit of material with a dominant mode in the 250 to 125μ (2ϕ to 3ϕ) range. This sediment is noticeably coarser than any other collected in the area from depths greater than 100 fathoms (183 m). Bottom photographs at this locality show a glacially rafted boulder or bedrock (Fig. 14a), a lag deposit (Fig. 14b) and a more typical bottom sediment (Fig. 15) near but not in the medial depression, indicating that the maximum intensity of the current is confined to the medial depression. Sediments collected on the sill flanks (Stations J-131 and J-143) were similar in grain size distribution. If the origin of the dominant mode in the 250 to 125μ (2ϕ to 3ϕ) range were the crest of the sill, a current velocity of at least 25 cm/sec. must flow in the medial depression. Slumping may carry the material derived from the crest to the flanks as the current velocity within the medial depression probably would not be maintained over the flanks. The two-way action of the current through the depression indicated by sediment parameters and size distribution curves, suggests a tidal origin.

Cumulative and frequency curves plotted for sediments collected on the sill along a line transverse to the medial depression (Fig. B-10, Appendix B) indicate very poor sorting, especially for samples collected immediately adjacent to the medial depression. The deeper the sample, the more dominant is the coarse fraction. This trend is the reverse of that shown in Figure B-9 (Appendix B). The very poor sorting and wide range of grain sizes indicate that the surficial sediments of the sill are probably of glacial origin and, with the exception of those sediments in the medial depression, have been little affected since initial deposition in Pleistocene time.

The distribution characteristics of sediments collected along the axis of the lower basin (Princess Royal Reach) is presented in Figure B-11 (Appendix B). The same two dominant modes of the upper basin (Fig. B-8, Appendix B) are apparent in sediments from the lower basin. However, the sediments in the lower basin originate from many sources whereas there is one dominant source in the upper basin.

Streams flowing into the sides of the lower basin contribute appreciable quantities of medium to fine sand (Fig. B-12, Appendix B) to the inlet margin. Additional evidence of multiple sources of sediment in the lower basin is the pronounced double mode in the silt-clay region of particle distribution which occurs not only at the upper end of the lower basin but also in sediments farther down the inlet (Fig. B-12, Appendix B).

Abundant shallow and mid-depth faunal remains were recovered from a depth of 285 fathoms (522 m) giving evidence of slumping within the lower basins (Fig. 16). Contributors to the shell debris are blue mussels (Mytilus edulis), brachiopods (Laqueus californicus vancouverensis), pelecypods (Thyasira cygnus and an unidentified pectin), scaphopods (Cadulus tolmei) and numerous solitary corals (Balanophyllia elegans and Caryophyllia alaskensis). In addition, numerous wood fragments were recovered and bottom photographs revealed a partially decomposed tree trunk embedded in the sediment.

Subsurface Sediment Characteristics

Four gravity cores (location shown on Fig. 17) were split and logged visually. The average sediment colour in the three cores from the upper basin was greyish olive (10Y/2). The core from the lower basin was a noticeably darker olive grey (5Y3/2). The majority of structures (Fig. 17) appear as slight changes in hue which were most visible just after the core had been split and the surface smear washed away. The average grain size of the cored sediment resembles the surficial sediment, i.e., the three collected in the lower part of the upper basin are silty clays, whereas the core from the lower basin is clayey silt with minor fine sand. Core J-123 contained three distinct, but thin, layers of fine sand and a two-foot layer of a green-grey clay. Core J-126 contained a single thin sand layer and a thinner green-grey clay layer. This clay is the only lithology that could be correlated to another core. E.V. Grill (oral comm.) has reported a green-grey clay on Patrick Sill below a depth of 12 to 24 inches (30 to 60 cm). The sand layers appear to be discontinuous lenses.

Wood fragments are the most abundant coarse material though unevenly distributed throughout the core. Generally the fragments occur with their long axes parallel or subparallel to the bedding indicating non-turbulent deposition. In Core J-123 the fragments were randomly oriented indicating

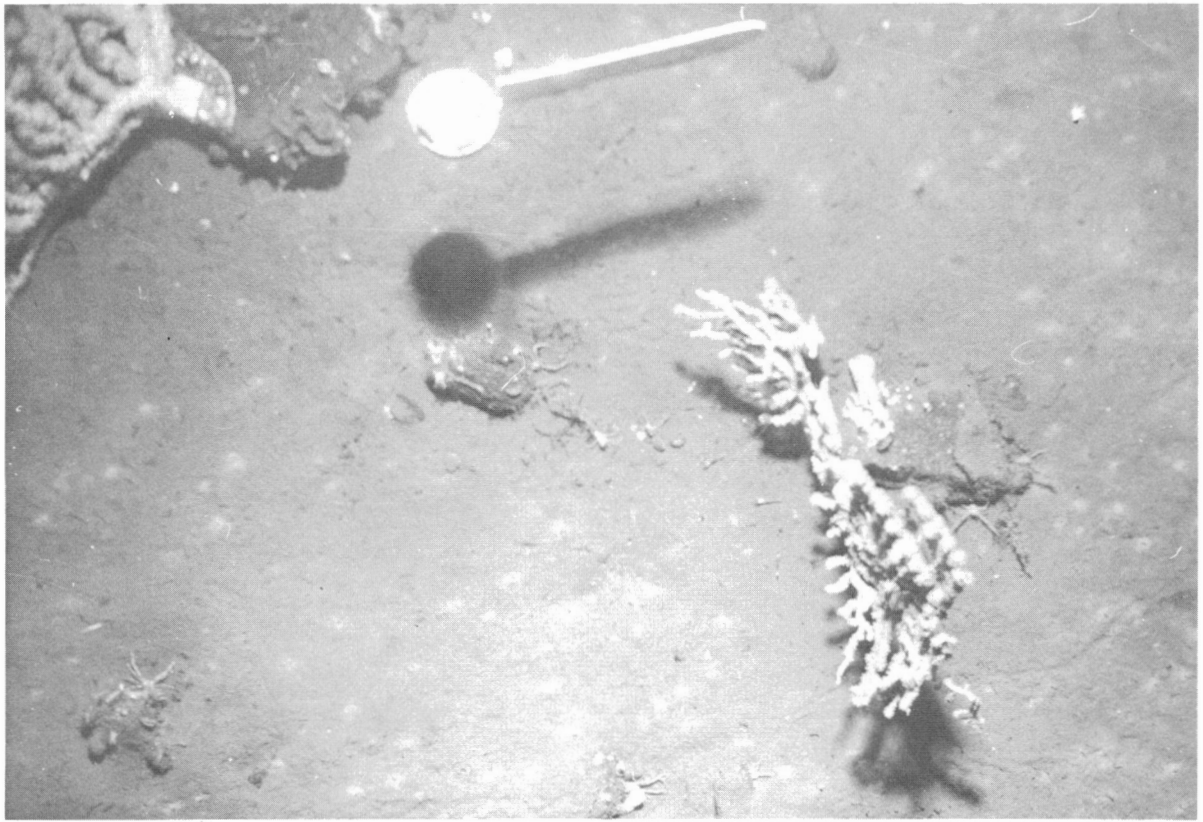

Figure 15. Bottom Photograph – Station J-19-67. Photograph taken on slope of medial depression to the east of the manganese concretion locality. A low sedimentation rate is indicated as well as minor influence of bottom currents. (about 1/8 x). GSC Photo No. 202279-E.

Figure 16. Bottom Photograph – Station J-160. Photograph taken in area where abundant shallow water faunal remains were recovered. (Depth = 285 fm or 522 m). Note disordered, hummocky topography. (about 1/8 x). GSC Photo No. 202279-F.

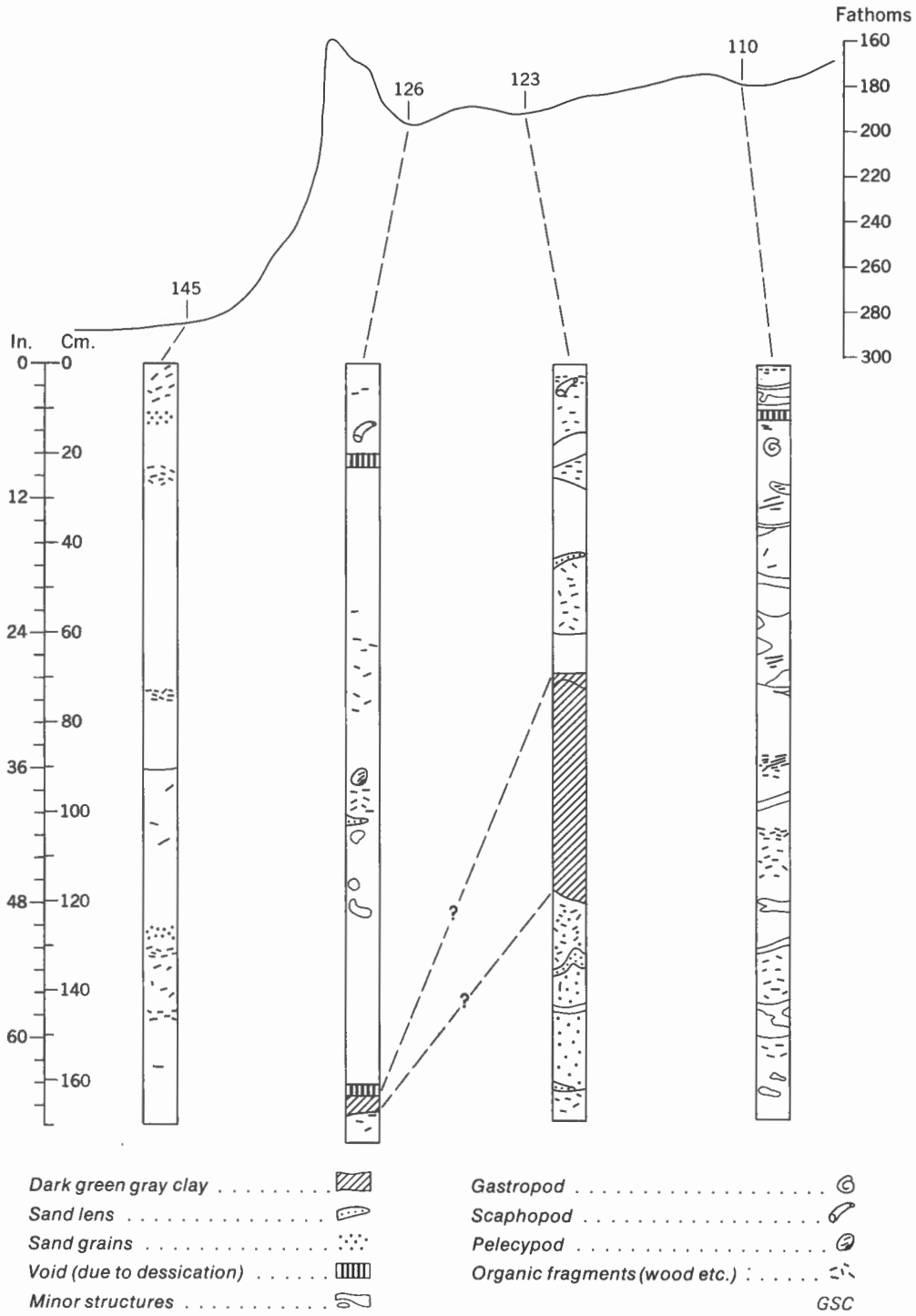

Figure 17. Gravity cores from upper Jervis Inlet.

turbulent deposition as in a slump. Recognizable shells and shell fragments consist of gastropods, scaphopods (Cadulus tolmei), and pelecypods (Thyasira cygnus). The latter species are the same as those recovered in the surficial sediment samples.

Summary of Jervis Inlet Sedimentation

Sediment is being transported to the basin floors of Jervis Inlet by several mechanisms. These include settling through the water column of fine-grained fluviatile material and periodic slumping of coarser grained material from the steep inlet walls with the possible initiation of turbidity currents. The optical turbidity data (Pickard and Giovando, 1960) indicate a major percentage (up to 50%) of suspendable material added to the inlet waters from the river at head is carried down the inlet within the low salinity surface waters. There is, however, a marked increase in turbidity in the bottom waters of the upper basin.

Slumping almost certainly occurs from the steep inlet walls which have an average slope of approximately 35 degrees. The abundance of shallow water faunal remains at the base of a steep submarine cliff in the lower basin support this concept. Other active areas are the large deltaic deposit off Malibu Rapids, and perhaps all the other smaller margin deltas which likely become unstable during periods of rapid sediment accumulation. Slumping is also believed to occur at the inlet head and on the south-facing flank of Patrick Sill where long unbroken slopes may result in the formation of turbidity currents.

Gravity cores collected within the upper basin were examined visually and revealed no distinctive graded bedding. However, the lack of orientation of elongate organic fragments within certain horizons in the cores suggest deposition under the turbulent conditions. Sand lenses within the cores taken from the upper basin likely represent the influence of slumping from the nearby inlet walls rather than from the inlet head.

There is a marked difference in grain size distribution between the upper and lower basins. Patrick Sill forms a boundary between these basins. To explain this depositional pattern, one must postulate either that the sill arrests the dominant depositional mechanism influencing the upper basin, or that the streams flowing into the lower basin have a much greater effect than those which flow into the upper basin. The relief of the sill is not sufficient to act as such an effective barrier if the majority of sediment is being added to the upper basin by the settling of particles through the water column. However, the sill is high enough that it would likely bar the passage of a turbidity current.

AUTHIGENIC MINERALS

Manganese Concretions

Source Area

Manganese concretions occur in the medial depression or "V"-notch on the south-facing slope of Patrick Sill (Fig. 18) at a depth of 175 to 190 fathoms (320-350 m) and cover an estimated 36,000 square yards (30,000 m^2) of the sea floor.

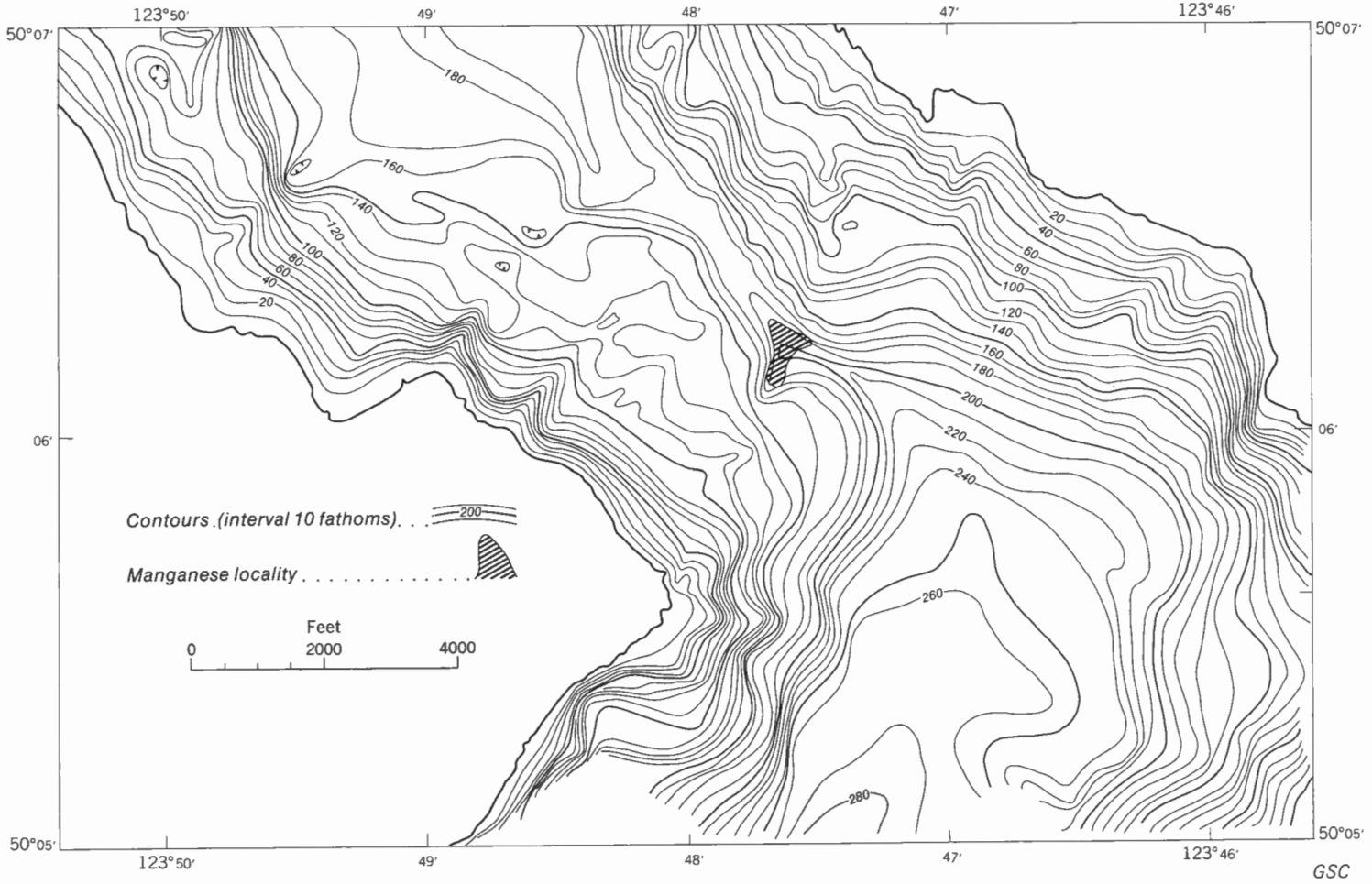

Figure 18. Bathymetry of Patrick Sill, Jervis Inlet (Northern portion).

The sediments collected with the concretions were generally similar to those found elsewhere within the area but, some samples recovered from the concretion locality showed the presence of a flocculant red-brown surface layer, one to several centimetres thick. The sediment within this layer often had a predominant coarse-grained component which is thought to represent a lag deposit. If the abundant fine sand noted at Station J-143 came from the concretion area, then the current within the "V"-notch must attain speeds of about 25 centimetres/second in order to move the sand. Underwater television observations of the locality substantiated the existence of a bottom current of approximately the velocity calculated. Bottom photographs taken on the sill show what appears to be a lag deposit (Fig. 14) associated with the concretions. Lag deposits are not evident in photographs taken near, but not on, the concretion locality. Apparently, the strongest currents in the area occur where the concretions are forming. Sedimentation rates here are correspondingly low. The total extractable iron and total carbon contents of the sediments recovered with the concretions were anomalously low. The low carbon content would reflect the sweeping away of the light organic material by the current. Figure 19 is a bottom photograph of the concretion locality.

Age and Growth Rates

The maximum age of the concretions would be determined by the time of ice retreat after the last major advance during the Pleistocene. This is estimated to be 12,000 B.P. (Armstrong et al., 1965). Evidence that the concretions formed in situ is provided by the recovery of siliceous sponges having a thick manganese-iron oxide coating. Also, the discoid shape and friable nature of the concretions precludes transport.

The maximum thickness of oxide material measured on any one concretion was 1.4 inches (35 mm). The accumulation rate of oxide material is highest in the horizontal plane. Assuming the age of the concretions to be 12,000 years, the apparent growth rate would be about .12 inch (3 mm)/1,000 years or less. This value is somewhat lower than the general accumulation rate of .4 to 40 inches (10 to 1,000 mm)/1,000 years suggested by Manheim (1965) for shallow marine concretions. However, Manheim (op. cit.) noted that concretion development in nearshore environments may be very irregular with wide variations over small areas. The porous nature and wide variation in lamination thickness of Jervis Inlet concretions suggests that the deposition rate was erratic, and, when deposition was occurring, much more rapid than the average rate of .12 inch (3 mm)/1,000 years.

Structure

The concretions occur in two distinct shapes – discoidal and spheroidal. Discoidal masses are usually larger and range up to 6 inches (15 cm) in diameter. Rock fragments, mostly granitic, form the nucleus of all specimens examined. The upper surfaces of the concretions are dark red-brown to brown, the under surfaces light yellow-brown. Brachiopods, serpulid worm tubes, bryozoan plates, siliceous sponges and corals may be attached to the upper surfaces.

The discoidal concretions frequently exhibit several interesting features. A side view (Fig. 20a) reveals the typical shape of this variety with a rock nucleus surrounded by a skirt of oxide material. The under surface of

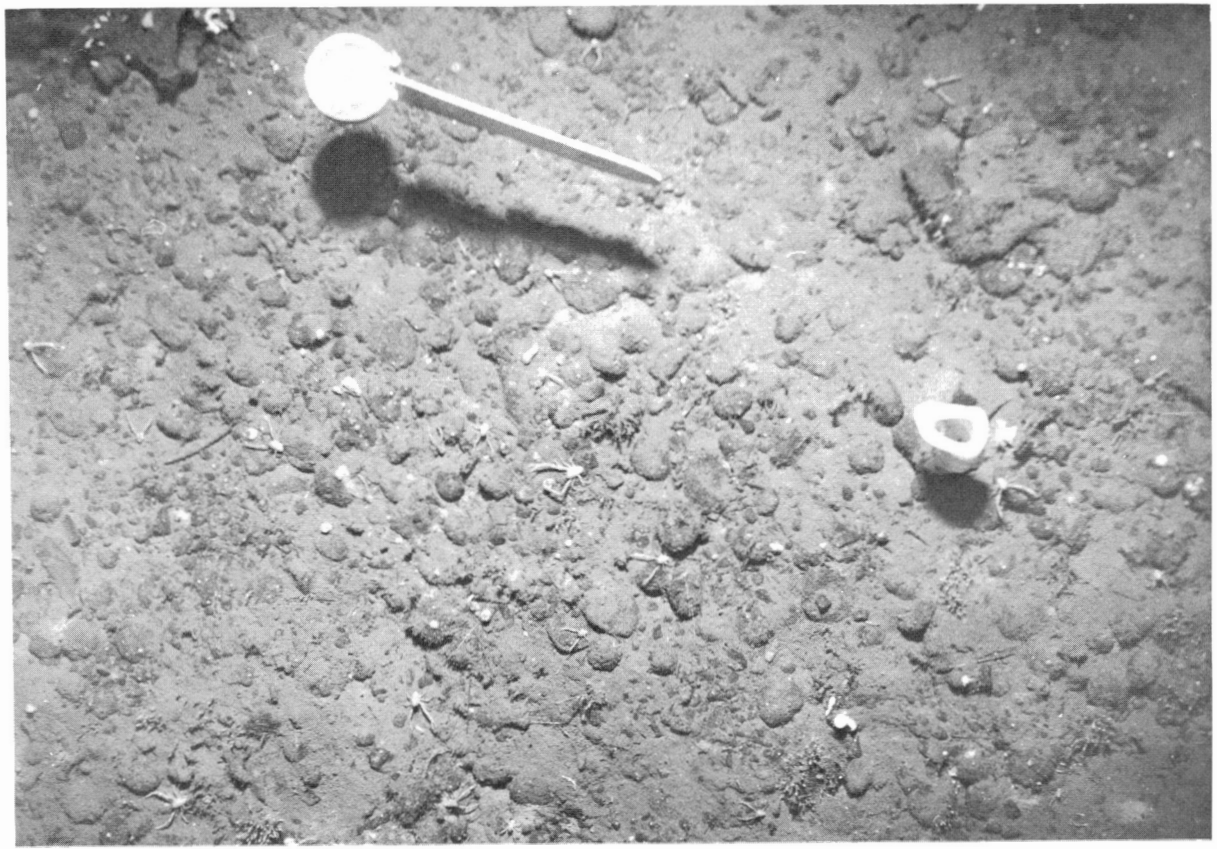

Figure 19. Bottom Photograph – Station J-19-67. Photograph taken on the manganese concretion locality. The rounded, exposed to partially buried masses are manganese concretions. Note general coarse texture of surficial sediments. (about 1/8 x). G.S.C. Photo No. 202279-G.

the skirt is usually even, and flat or concave downwards in contrast to the upper surface which is often very irregular. Some specimens of discoidal concretions have apparently been rotated about a horizontal axis at one time during their formation. On one side of the nucleus the oxides have accumulated in two lobes or skirts to form a lip-like structure while the opposite side of the nucleus is nearly devoid of oxides. Oxide materials are apparently deposited about a nucleus in a plane paralleling the sediment-water interface. The asymmetry in plan view of the oxide skirt of many of the specimens indicates a favoured direction for greatest growth. This orientation is also exhibited by the oxide crusts which have formed as plateaus on dead siliceous sponges which have toppled.

The nuclei of spheroidal concretions are completely enclosed by oxides. The difference between spheroidal and discoidal types may be due in part to the size and shape of the nucleus. The generally smaller and more equidimensional nuclei of the spheroidal types perhaps allow these to be rolled about the bottom by currents or animals. Figure 20b shows two spheroidal masses which have coalesced with the formation of a surrounding skirt. Since coalescense, this mass has behaved as a discoidal concretion.

Cross-sections of manganese concretions studied in polished section (Sorem, 1967) are illustrated on Figure 21. The thinner, dark laminations correspond to finer grained material, and are generally enriched in the metallic oxides and contain few detrital minerals. The thicker, lighter coloured laminations include most of the detrital sediment, dominantly quartz and feldspar as in the underlying sediments. Apparently the darker layers represent periods of slow deposition. In vertical sections the laminations are shown to be approximately symmetrical about a horizontal plane.

Chemical Composition

The chemical composition of the manganese concretions (Table 5, Appendix A) has been determined by Grill et al. (1968). The compositions of deep ocean, Baltic Sea and Vermilion Sea (off Baja California) concretions (Table 6, Appendix A) are presented for comparative purposes (Manheim, 1965; Mero, 1965).

Total carbon analyses of Jervis Inlet concretions indicated values (1.26%) equal to or slightly less than the underlying sediments.

The ratio of manganese to iron has been correlated with depth and used in an attempt to distinguish and classify concretion localities (Mero, 1965). These ratios can be extremely variable with a considerable range sometimes occurring within a single specimen. In general, concretions from neritic and lake environments have a Mn/Fe ratio of less than unity. A majority of pelagic nodules have a ratio of greater than unity. Jervis Inlet concretions have an average Mn/Fe ratio of 5, there being little variation between samples. While this ratio does not follow the norm for shallow water concretions, it is by no means unique. Some nodules close to the North and South American coasts and near Japan have Mn/Fe ratios ranging from 12 to 50 (Price, 1967). The more analyses that are published, the less evident becomes the supposed relationship between depth and Mn/Fe ratio.

The oxidation state of the manganese was calculated (Grill, Murray and Macdonald, 1968) to be $MnO_{1.87}$ for sample A and $MnO_{1.86}$ for sample B, assuming all the active oxygen was associated with higher oxides of manganese. This O/Mn ratio is somewhat higher than the average value for neritic

areas (1.55) and lower than that for the pelagic areas (1.9 - 2.0) (Manheim, 1965). Unlike the Mn/Fe ratio, the O/Mn ratio apparently has a significant covariance with depth (Manheim, op. cit.). However, a considerable overlap of O/Mn ratios exists between shallow- and deep-water concretions.

The minor element content of Jervis Inlet concretions (Grill, Murray and Macdonald, 1968) approximates other neritic occurrences. Elements of economic concern such as Cu, Ni, Zn and Co have abundances ranging from 1 to 2 orders of magnitude below the estimated deep ocean average. Lead was not detected while molybdenum occurred with an abundance similar to that of deep sea concretions. The original analyses (Grill, Murray and Macdonald, op. cit.) were given as oxide percentages of the soluble and insoluble (in a heated solution containing 10 ml of hydrochloric acid and 10 g of hydroxylamine hydrochloride) fractions. The major elements in the insoluble fraction were silicon, aluminum, iron, calcium, magnesium and sodium. These likely formed the detrital silicate minerals which were included within the ferromanganese oxide crusts. The phosphorus content of manganese concretions is thought to be related to their association with semi-stagnant sediments. Jervis Inlet concretions contained approximately 0.3 per cent phosphorus which is common for shallow marine occurrences. Tellurium was detected in the soluble fractions of both the Jervis Inlet samples analyzed.

Mineralogy

Todorokite was identified as the principal manganese mineral in Jervis Inlet concretions (Grill et al., op. cit.). The suggested composition (Straczek et al., 1960) is: $(Ca, Na, Mn^{+2}, K)(Mn^{+4}, Mn^{+2}, Mg)_6O_{12}.3H_2O$. Calculations of atomic proportions (the number of atoms per unit cell) of Mn^{+4}, Mn^{+2}, Mg (including Co, Cu), Ca (including Ba, Sr), Na and K for soluble Jervis Inlet material agrees with similar data presented for todorokite (Grill et al., op. cit.).

Formation of Concretions

The mechanism of formation of manganese concretions can only be postulated. Many workers (Manheim, 1965; Price, 1967) consider the growth of concretions to be due to the precipitation of elements from the interstitial waters of underlying sediments. Metals present in low concentrations in sea water are deposited as oxides or as ions adsorbed on clay and organic particles. Release of these metals to the interstitial waters would occur with sediment burial due to the reducing effect of the organic matter. The resulting high concentration of elements in the interstitial waters as well as electrochemical differences between the adjacent reducing and oxidizing environments will set up a diffusion potential so causing the upward movement of these elements (Price, 1967).

This mechanism could produce a variety of concretion habits. Manheim (1961) suggested that in areas where the sediment-water interface is neutral or reducing, nodules will not form but the trace-element content of the bottom waters will be increased. Conversely, in areas where the surficial sediments are highly oxidized, pea ores may form within the sediment itself (Gripenburg, 1934).

Although the basic mechanisms for the formation of concretions in the shallow water and open ocean environments are believed similar, the concentration of many minor metals such as Cu, Co, Ni, Pb and Zn is one to

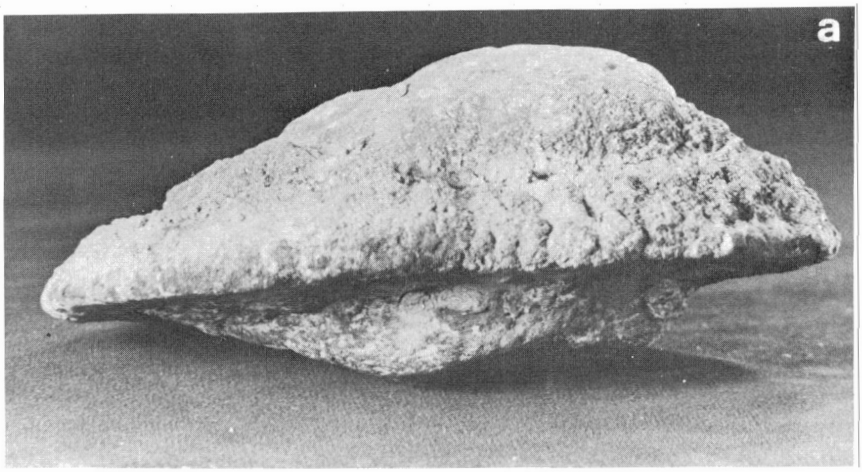

a. Side view of a large discoidal manganese concretion. The nucleus is a granitic boulder. Major diameter 5.5 inches (13.1 cm). G.S.C. Photo No. 202279-H.

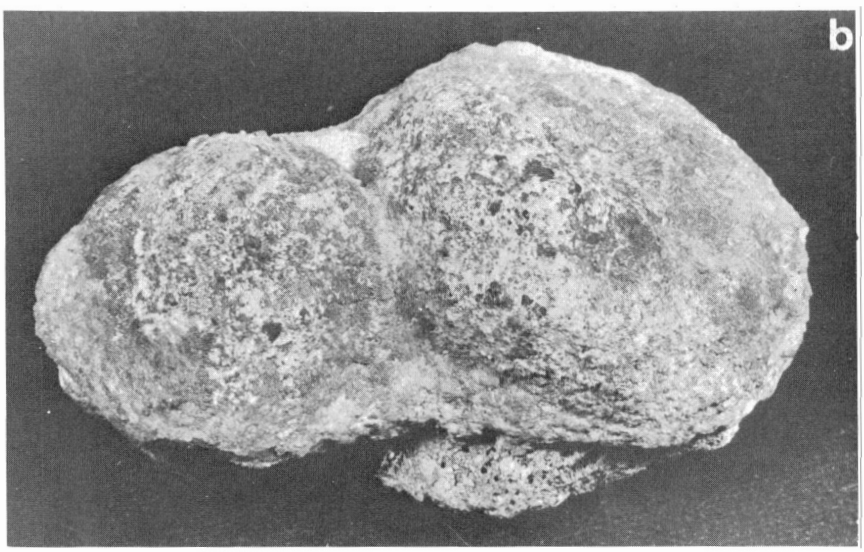

b. Coalescence of two discoidal concretions. Major diameter about 3 inches (7.5 cm). G.S.C. Photo No. 202279-I.

Figure 20. Examples of Manganese Concretions.

several orders of magnitude less in shallow than in the deep ocean varieties. This is believed to be due to differing concentrations and types of organic matter present in the two environments (Price, 1967). In neritic and lacustrine conditions, burial of the sediment and reduction in the presence of organic material releases most Mn, Pb and Zn to the interstitial waters while the loss of Fe, Ni, Co and Cu is smaller and possibly due to retention of these elements in iron sulphides (Price, op. cit.). Water soluble organics, amino acids and humic acids within the sediments are also thought to affect metal concentrations of shallow water concretions by modifying the inorganic uptake of minor metals such that Ph, Zn and Cu are not sorbed by the manganese-iron phases. In the open ocean environment the low abundance of organic matter in the sediments would likely minimize the mobility and upward diffusion of manganese and other elements during sediment burial.

Abundance and Value

The total air dried weight of the concretions recovered from 0.2 square yard (0.17 m^2) was 1.97 pounds (.894 kg) of which 72.9 per cent or 1.43 pounds (.684 kg) was oxide material. The concentration of oxide material would be 7.1 pounds/square yard (3.9 kg/m^2). If the area of the deposit is taken to be 36,000 square yards (30,000 m^2) the tonnage of oxides present would be 128 short tons (117 metric tons). This estimate could be in error by a considerable amount (perhaps ±50 per cent) since only one sample was weighed and taken to represent an average sample of the entire area.

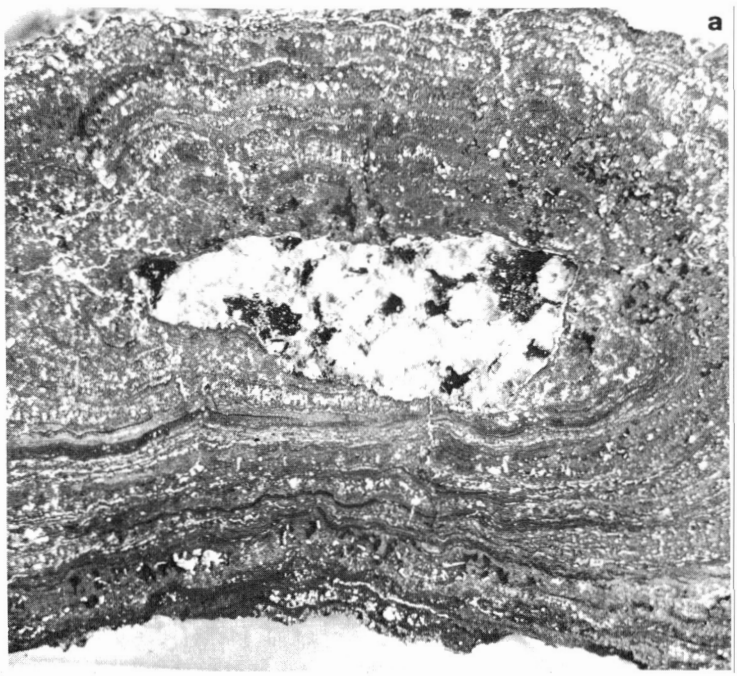

Figure 21 a. Cross-section of middle portion of discoidal concretion which had nucleus completely enclosed by oxide materials (about 4.3 x). Early layers of oxides were preferentially deposited on left side of nucleus as it appears in the photograph. GSC Photo No. 202279-J.

While the above method of determining reserves of authigenic oxides on Patrick Sill is accurate within itself, many similar samples will have to be taken in order to estimate reasonably accurately the total tonnage. Underwater television was tried as a method to determine concentrations but concretions could not be distinguished from barren boulders with the system available.

Iron Crusts

Maintaining station over the concretion locality was difficult and only about half of the attempts to obtain samples were successful. One attempt, which proved to be too far to the west by about 100 to 200 feet resulted in the sampler hitting either bedrock or very large boulders. However, within the grab sampler were ferruginous crusts (Fig. 22) which had been broken off the rock surface.

The external surfaces of the crusts vary smooth to irregular. Cross-sections reveal a distinct layering. The surface or outer layer is rind-like and varies in thickness from about .04 to 0.6 inch (1 to 15 mm). The colour is red-brown to dark brown and black. The material is non-porous and has a vitreous to opaline lustre as if deposited as a gel. On desiccation at room temperature the thicker portions have cracked forming interlocking polyhedral masses. Deposition of the gel-like material must have occurred reasonably rapidly as large bubble-like cavities were formed (Figs. 22b, c). The principal mineral forming this outer layer is goethite (FeOOH).

The bulk of the material forming the crust is reddish yellow to yellow-brown, fine grained, loose and very porous. An X-ray powder diffraction pattern indicated the principal minerals to be quartz, feldspar and goethite. This material likely represents sediments which accumulated and were then

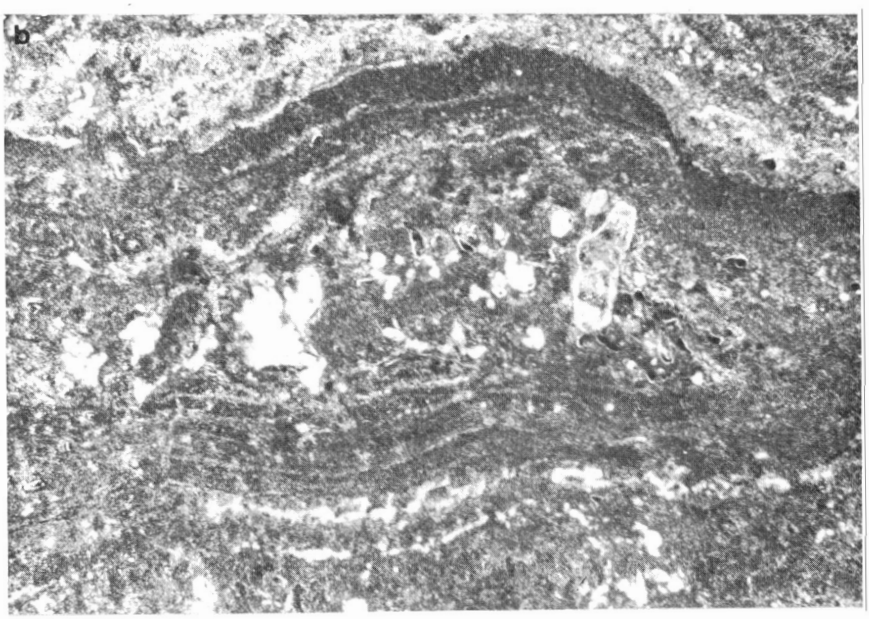

Figure 21 b. Enlargement from concretion pictured in 'a' showing detritial mineral included in accreted oxide materials. Detritial minerals are generally most abundant in the porous, lighter coloured oxide layers (about 43 x). GSC Photo No. 202279-K.

Figure 21. Cross Sections of Manganese Concretions.

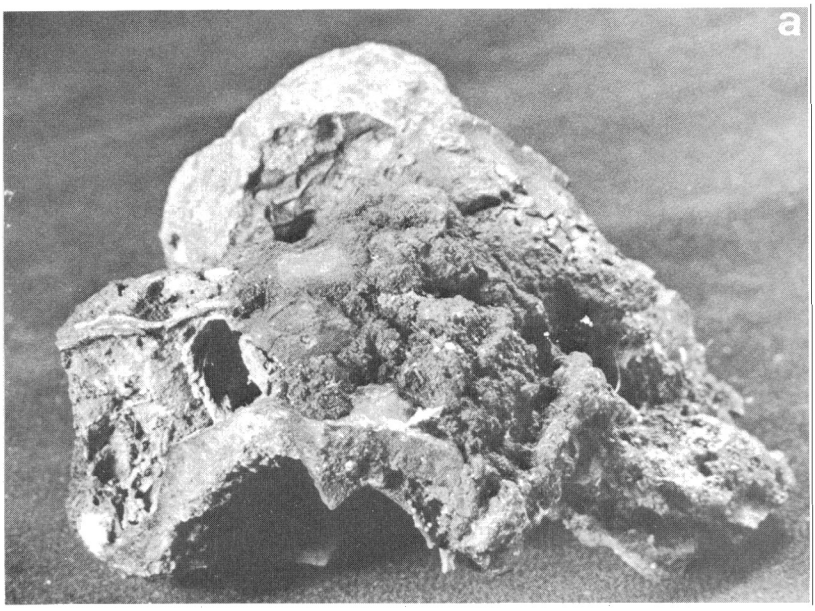

Figure 22 a.

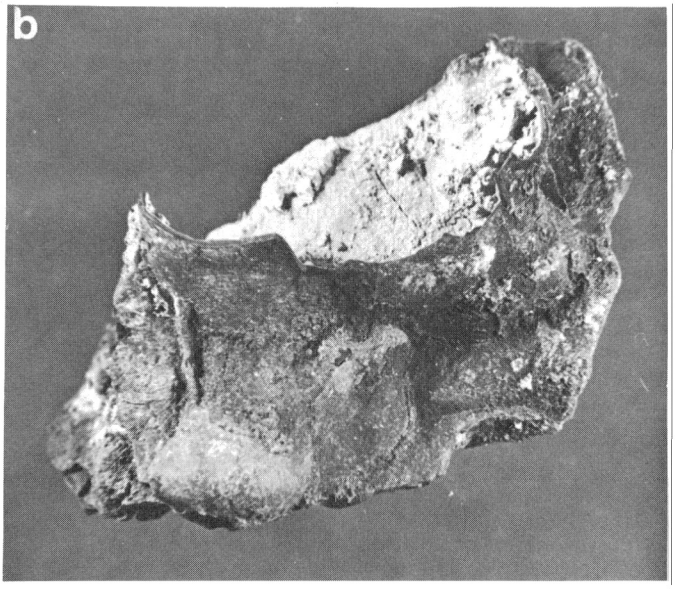

Figure 22 b.

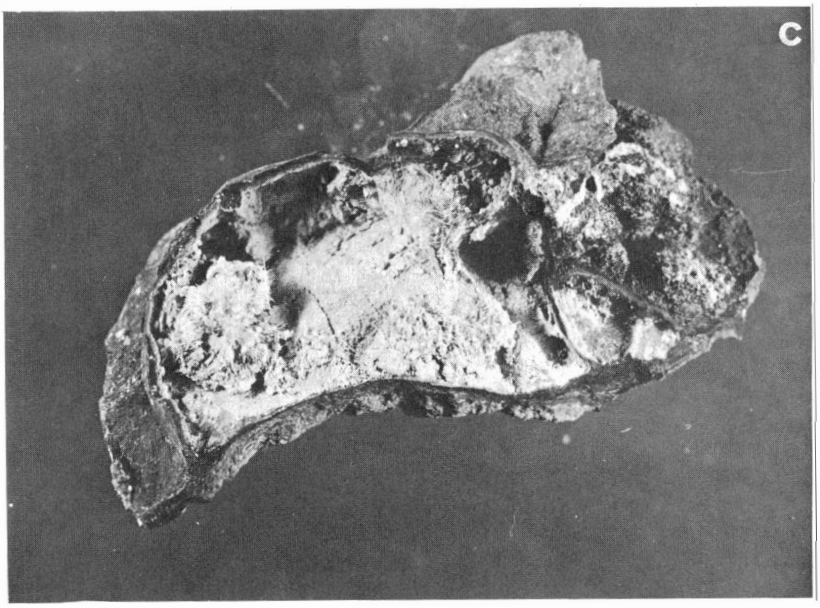

Figure 22 c.

a. Iron crust as recovered from rock face near but not on (i.e. within about 100 metres) the concretion locality. (about 1.6 x). GSC Photo No. 202279-L.

b, c. Bubble-like structure shown by some of the iron crusts recovered from vicinity of concretion locality. Note layering within material of bubble and base fragments of sponges within bubble. (about 1.6 x). GSC Photo Nos. 202279-M, 202279-N.

Figure 22. Iron crusts from Patrick Sill.

included in the structure of the crusts by the deposition of the gel-like material. The layering mentioned is due to alternating layers of loose, porous and vitreous materials. The nature of the material which formed the bond with the rock surface is not known.

There is no feature of the crust which would give an indication of age.

"Glauconite-Montmorillonoid" Pellets

Murray and MacIntosh (1968) described interstratified glauconite-montmorillonoid pellets from Queen Charlotte Sound. Mineralogic and morphologic studies of Jervis Inlet sediments revealed the presence of physically identical pellets (Fig. 10b). These pellets were found over a considerable area of the sill as well as in localized areas on the sides of the lower basin. Pellets were not noted in samples collected from the upper basin. No X-ray or chemical analyses have been made of these pellets to date.

The pellets are generally spheroidal and light yellow-green to grey-green in colour. In the fractions examined, the pellets are most abundant in the fine sands (i.e. 88 to 63μ or 3.5 to 4Ø) but some samples contained pellets in the 500 to 350μ (1.0 to 1.5Ø) range. Both these fractions of sample J-135, which is near but not on the concretion locality, were estimated to be 40 per cent pellets. The finer fraction of sample J-164 was also about 40 per cent pellets. Sediments collected with concretions were about 15 per cent pellets for the fractions examined. Often recovered with the pellets were sponge spicules and radiolarian tests.

Discussion

Speculative conclusions can only be made as to why manganese concretions and iron crusts are forming on Patrick Sill and apparently not elsewhere within upper Jervis Inlet. The area of the medial depression is affected by a bottom current with an approximate velocity of 25 centimetres/second. This current limits the deposition of detritus, both minerogenic and organic, and in some areas is capable of winnowing, with subsequent formation of lag deposits. The surficial sediments of the concretion locality are a dark red-brown colour for a depth of about 1 to 2 centimetres. Below this layer the sediments are generally a typical olive-green. The colour of the surficial sediments indicates oxidizing conditions probably due to the constant renewal of overlying waters and the lower organic matter content of the sediments.

Iron is being deposited as goethite crusts on exposed rock surface within the medial depression of the sill. Apparently simultaneously and in close proximity, manganese concretions are forming around rock fragments resting on sediments. Whereas the source of the goethite is likely a gel formed in the sea water, the concretion-forming manganese is believed, derived from the substrate.

"Glauconite-montmorillonoid" pellets are also forming within upper Jervis Inlet, but they are not unique to the sill. Certain samples collected from the wall of the lower basin contained these pellets in considerable quantity, but no pellets were found in the sediments of the upper basin. Whether these pellets form on or beneath the sediment-water interface is unknown.

Exploration

If, in the future, the mining concentrations of shallow marine concretions becomes profitable, the question will arise as to how to locate these deposits. At present, the best guide would probably be bathymetry. Favourable conditions appear to be achieved on the crests of banks and sills or on basin margins. All presently known local occurrences of concretions have been found in the 100- to 200-fathom range. However, the significance of depth is not known. Movement of the overlying waters is needed to maintain a low sediment accumulation rate and oxidizing conditions within the bottom waters and top centimetre or so of the sediments. The occurrence of a stagnant to semi-stagnant basin adjacent to the elevated area is considered important (Price, 1967). To date, not enough is known about trace element concentrations within sea water and sediment in areas where concretions form to enable one to use such data for exploration.

REFERENCES

Armstrong, J.E., Crandell, D.P., Easterbrook, D.J., and Noble, J.B.
1965: Late pleistocene stratigraphy and chronology in southwestern British Columbia and Northwestern Washington; Geol. Soc. Am. Bull., v. 76, p. 321-330.

Bacon, W.R.
1957: Geology of lower Jervis Inlet; Brit. Columbia Dept. Mines Petrol. Resour., Bull. 39.

B.C. Natural Resources Conference
1956: British Columbia Atlas of Resources.

Canadian Tide and Current Tables
1969: Juan de Fuca and Georgia Straits; Canadian Hydrographic Service, v. 5, Dept. Environment, Ottawa, Ontario.

Cockbain, A.E.
1963: Distribution of sediments on the Continental Shelf off the southern B.C. coast; Ms Rept. 15, Inst. Oceanogr., Univ. Brit. Columbia, Vancouver, B.C.

Dobrin, M.B.
1960: Introduction to geophysical prospecting; McGraw-Hill, 446 p.

Folk, R.L.
1961: Petrology of sedimentary rocks; Univ. Texas, 154 p.

1966: A review of grain size parameters; Sedimentology, v. 6, p. 73-93.

Folk, R.L., and Ward, W.C.
1957: Brozos River bar, a study in the significance of grain size parameters; J. Sediment. Petrol., v. 27, p. 3-27.

Grill, E.V., Murray, J.W., and Macdonald, R.D.
1968: Todorokite in manganese nodules from a British Columbia fjord; Nature, v. 129, no. 552, p. 358-359.

Grim, R.E.
1968: Clay mineralogy; McGraw-Hill, 596 p.

Gripenburg, S.
1934: A study of sediments of the North Baltic and adjoining seas; Hausforskningsinstitutets Skrift, v. 96, p. 1-231.

Gucleur, S.M., and Gross, M.S.
1964: Recent marine sediments in Saanich Inlet, a stagnant marine basin; Limnol. Oceanogr., v. 9, no. 3, p. 359-375.

Holland, S.S.
1964: Landforms of British Columbia; Brit. Columbia Dept. Mines Petrol. Resour., Bull. 48.

Kindle, E.M.
1932: Lacustrine concretions of manganese; Am. J. Sci., v. 24, p. 496-504.

Kittrick, J.A., and Hope, E.W.
1963: A procedure for the particle size separation of soils for X-ray diffraction analysis; Soil Sci., v. 96, p. 319-325.

Lazier, J.R.N.
1963: Some aspects of the oceanographic structure in the Jervis Inlet system; unpubl. M.Sc. thesis, Univ. Brit. Columbia, Vancouver, B.C.

LeRoy, O.E.
1908: Preliminary report on a portion of the main coast of British Columbia and adjacent islands; Geol. Surv. Can., Rept. no. 996.

Macdonald, R.D.
1970: Marine geology of upper Jervis Inlet; unpubl. M.A.Sc. thesis, Univ. Brit. Columbia, Vancouver, B.C.

Manheim, F.T.
1961: A geochemical profile of the Baltic Sea; Geochim. Cosmochim. Acta, v. 25, p. 52-71.

1965: Manganese-iron accumulations in the shallow marine environment; symposium on marine geochemistry, Narragansett Marine Laboratory, Univ. Rhode Island, Occas. Publ. no. 3, p. 217-275.

Mero, J.L.
1965: The mineral resources of the sea; Elsevier Publishing Co., 312 p.

Murray, J.W., and Mackintosh, E.E.
1968: Occurrence of interstratified glauconite-montmorillonoid pellets, Queen Charlotte Sound, British Columbia; Can. J. Earth Sci., v. 5, p. 243-247.

Pantin, H.M.
1969: The appearance and origin of colours in muddy marine sediments around New Zealand; New Zealand J. Geol. Geophs., v. 12, no. 1, p. 51-56.

Peacock, M.A.
1935: Fjord-land of British Columbia; Geol. Soc. Amer. Bull., v. 46, p. 633-696.

Pickard, G.L.
1956: Physical features of British Columbia inlets; Roy. Soc. Can. Trans., L(III), p. 47-58.

1961: Oceanographic features of inlets in the British Columbia mainland coast; J. Fisheries Res. Board Can., v. 18, no. 6, p. 907-999.

Pickard, G.L., and Giovando, L.F.
1960: Some observations of turbidity in British Columbia inlets; Limnol. Oceanogr., v. 5, no. 12, p. 162-170.

Pickard, G.L., and Rodgers, G.K.
1959: Current measurements in Knight Inlet, British Columbia; J. Fisheries Res. Board Can., v. 16, p. 635-678.

Porrenga, D.H.
1967: Glauconite and chamosite as depth indicators in the marine environment; Marine Geol., v. 5, p. 495-501.

Price, N.B.
1967: Some geochemical observations on manganese-iron oxide nodules from different depth environments; Marine Geol., v. 5, p. 511-538.

Roddick, J.A.
1965: Vancouver north, Coquitlam and Pitt Lake map-areas; Geol. Surv. Can., Mem. 335, 376 p.

Shepard, F.P.
1954: Nomenclature based on sand-silt-clay ratios; J. Sediment. Petrol., v. 24, p. 151-158.

Sorem, R.K.
1967: Manganese nodules: Nature and significance of internal structure; Econ. Geol., v. 62, no. 1, p. 141-147.

Sorem, R.K., and Foster, A.R.
1972: Marine manganese nodules: Importance of structural analysis; 24th Int. Geol. Cong. Sec. 8, Marine Geology and Geophysics, p. 192-200.

Straczek, J.A., Horen, A., Ross, M., and Warshaw, C.M.
1960: Studies of manganese oxides, IV. Todorokite; Amer. Mineral., v. 45, p. 1174-1184.

Strøm, D.M.
1936: Land-locked waters. Hydrography and bottom deposits in badly ventilated Norwegian fjords with remarks upon sedimentation under anaerobic conditions; Skr. Norske Uidensk, Akad. Oslo, v. 1, no. 7, p. 1-85.

Tiffin, D.L., and Murray, J.W.
1966: Mapping offshore with continuous seismic; Oil Week, Nov. 7, 1966.

Toombs, R.B.
1956: Bute Inlet sediments; Roy. Soc. Can. Trans., Ser. III, v. 50, p. 59-65.

Trask, P.D.
1938: Organic content of recent marine sediments, in Recent Marine Sediments - A symposium; Amer. Assoc. Petrol Geol., Denver, Colorado, p. 736.

Trites, R.W.
1955: A study of the oceanographic structure in British Columbia inlets and some of the determining factors; Ph.D. thesis, Univ. Brit. Columbia, Vancouver, B.C.

Weaver, C.E.
1958: Geologic interpretation of argillaceous sediments, Part I, origin and significance of clay minerals in sedimentary rocks; Amer. Assoc. Petrol. Geol. Bull., v. 43, no. 2, p. 254-271.

APPENDIX A

TABLES 1 to 6

Table 1. Time stratigraphic units for Pleistocene of southwestern British Columbia (after Armstrong et al., 1965)

1) Salmon Springs Glaciation >37,000 years B.P.

2) Olympia Interglaciation <24,500 > 15,000 - 37,000 years B.P.

During this period, ice was absent from the lowlands of southwestern British Columbia.

3) Fraser Glaciation approx. 9,500 - 15,000 <25,000 years B.P.

This glaciation is probably the regional equivalent of the Wisconsin Glaciation of the mid-western United States.

a) Evans Creek Stade 17,000 - 25,000 years B.P.

By definition, during this period, large alpine glaciers formed and reached their maximum extent. In British Columbia, expansion of the glaciers apparently resulted in ice sheet formation.

b) Vashon Stade 13,000 - <21,000 >15,000 years B.P.

By definition, the Vashon is the last major climatic episode during which drift was deposited by continental ice originating in British Columbia, and occupying the lowlands of southwestern British Columbia and northwestern Washington.

c) Everson Interstade 11,000 - 13,500 years B.P.

This period began with the invasion of the lowlands by the sea, and ended with either the advance of the Sumas ice sheet or the withdrawal of the sea and the disappearance of the floating ice.

d) Sumas Stade 9,500 - 11,000 years B.P.

A climatic episode during final stages of emergence of the Fraser Lowland when a valley glacier occupied the eastern part of the lowland. This glacier may have been only a local advance of the Cordilleran ice sheet.

Table 2. Mineral abundances in fine sand fraction (by per cent)

Sta. No.	Quartz	Feldspar			Micas		Amphibole	Pyroxene		Epidote	Magnetite	Apatite	Unidentified and Misc.
		K	Plag.	Indet.	Chlorite	Biotite		Clino.	Ortho.				
101	20.0	4.6	35.5	7.9	2.9	0.9	15.9	0.8	0.5	6.6	1.3	-	3.0
102	23.8	4.4	31.9	13.1	8.0	3.0	12.5	1.0	0.5	3.1	0.1	0.1	3.1
103	27.0	10.4	29.0	7.5	7.1	2.2	7.4	0.5	0.3	2.9	0.4	-	5.2
104	32.6	9.8	21.4	8.5	2.5	4.1	10.5	0.5	0.1	3.0	0.3	0.6	4.4
105	27.7	7.2	21.5	8.5	13.1	4.3	12.2	0.1	-	3.7	1.0	0.1	1.9
108	19.3	2.6	15.5	6.4	2.1	4.1	28.9	0.8	2.0	12.7	1.2	0.4	4.9
109	21.1	5.1	42.1	8.9	9.1	4.8	8.2	1.8	0.3	1.7	1.1	0.2	1.0
110	24.8	8.0	34.8	9.6	-	-	-	-	-	-	-	-	-
118	18.9	8.0	50.0	3.3	8.2	1.2	6.0	0.2	1.0	0.3	0.7	-	2.1
19-67	22.6	5.7	41.5	9.3	9.9	2.2	5.0	0.1	0.2	1.0	0.7	-	1.9
126	23.8	6.7	49.5	4.3	4.4	4.9	4.1	0.2	0.4	0.3	0.3	0.1	1.0
132	29.8	3.6	46.1	1.6	2.5	10.4	3.1	-	0.3	0.5	0.2	-	1.8
138	20.8	7.2	44.2	5.7	3.3	8.2	5.7	-	0.4	1.7	0.3	-	2.6
147	18.7	5.5	41.6	2.5	13.4	13.4	2.3	-	0.1	0.6	0.1	-	2.0
155	23.5	12.6	40.3	6.3	8.9	3.5	3.2	-	0.2	0.3	0.2	-	0.9

Table 3. [001] Peaks (in Angstroms) of minerals in clay size fraction

	TREATMENT				
MINERAL	K	K 300°C	K 500°C	Mg	Mg and Glycerol
Chlorite	14	14.2	14.2	14.2	14.2
Illite	10	10	10	10	10
Vermiculite	10-13	10	10	14-15	14
Montmorillonite	12-14	10	10	12.8-14	17-18
Illite-montmorillonite	10-14	10	10	10-14	10-18
Illite-vermiculite	10-13	10	10	10-15	10-14
Illite-chlorite	10-14	10-14	10-14	10-14	10-14
Plagioclase	3.18	3.18	3.18	3.18	3.18
Quartz	3.3	3.3	3.3	3.3	3.3
Amphibole (hornblende)	8.40	8.40	8.40	8.40	8.40
K-feldspar	3.24	3.24	3.24	3.24	3.24

Table 4. Relative abundances of clay mineral species

J-101	Illite	3-4	J-102	Fe chlorite	4	J-103	Fe chlorite	3-4	J-104	Mg-Fe chlorite	4
	Fe chlorite	3-4		Illite-montmor.	3		Illite	3-4		Illite	3-4
	Illite-montmor.	3-4		Illite	3		Vermiculite	3		Vermiculite	3
	Montmorillonite	3		Montmorillonite	3		Illite-vermic.	3		Vermic.-illite	3
	Amphibole	2		Plagioclase	2		Plagioclase	2-3		Plagioclase	2
	Plagioclase	2		Amphibole	2		Quartz	2-3		Quartz	2
	Quartz	2		Quartz	2		Amphibole	2		Amphibole	2
J-105	Fe chlorite	3-4	J-108	Fe chlorite	4	J-109	Mg-Fe chlorite	4	J-110	Mg-Fe chlorite	3-4
	Illite	3-4		Illite	3-4		Illite	3-4		Vermiculite	3-4
	Vermiculite	3-4		Vermiculite	3		Vermiculite	3		Illite-vermic.	3-4
	Illite-vermic.	3		Illite-vermic.	3		Illite-vermic.	3		Illite	3
	Plagioclase	2		Plagioclase	2		Plagioclase	2		Plagioclase	2
	Quartz	2		Quartz	2		Quartz	2		Quartz	2
	Amphibole	2		Amphibole	2		Amphibole	2		Amphibole	2
							Illite-chlorite	2			
J-118	Mg-Fe chlorite	3-4	J-123	Mg-Fe chlorite	4				J-19-67	Vermiculite	3-4
	Illite	3-4		Illite	3-4	J-126	Vermiculite	4		Fe chlorite	3-4
	Vermiculite	3-4		Vermiculite	3-4		Mg-Fe chlorite	3		Illite	3
	Illite-vermic.	3		Illite-vermic.	2-3		Illite	3		Illite-vermic.	2-3
	Plagioclase	2		Illite-chlorite	2		Illite-vermic.	3		Quartz	2
	Quartz	2		Quartz	2		Quartz	2		Plagioclase	2
	Amphibole	2		Plagioclase	2		Illite-chlorite	2		Amphibole	2
	Illite-chlorite	2		Amphibole	2		Plagioclase	2		Illite-chlorite	2
							Amphibole	2			
J-132	Fe chlorite	4	J-138	Fe chlorite	3-4				J-155	Fe chlorite	3-4
	Vermiculite	3-4		Illite	3-4	J-147	Vermiculite	4		Illite	3-4
	Illite	3		Vermiculite	3		Mg-Fe chlorite	3-4		Vermiculite	3-4
	Illite-vermic.	2-3		Illite-vermic.	2-3		Illite	3-4		Illite-vermic.	2-3
	Quartz	2		Illite-chlorite	2		Illite-vermic.	2-3		Quartz	2
	Plagioclase	2		Quartz	2		Plagioclase	2		Plagioclase	2
	Amphibole	2		Plagioclase	2		Quartz	2		Amphibole	2
	Illite-chlorite	2		Amphibole	2		Amphibole	2		Illite-chlorite	2
							Illite-chlorite	2			

Scale of abundance

5	Dominant	65 - 100%
4	Major	35 - 65%
3	Minor	10 - 35%
2	Trace	0 - 10%
1	None	

Table 5. Chemical analyses of Jervis Inlet concretions (after Grill, Murray and Macdonald, 1968)

Sample	A*		B	
% Soluble	81.75		81.09	
Fraction	Soluble	Insoluble	Soluble	Insoluble
Fe_2O_3	7.65	3.06	6.55	2.45
FeO	-	1.79	-	1.23
MnO	51.70	0.10	52.31	0.10
SiO_2	2.3	64.9	-	67.1
Al_2O_3	0.41	15.8	0.71	15.3
TiO_2	0.096	0.62	0.085	0.58
P_2O_5	0.94	0.11	0.72	0.16
Na_2O	1.06	2.27	1.05	2.37
K_2O	1.11	1.52	1.18	1.51
MgO	3.19	2.24	3.36	1.66
CaO	1.55	3.19	1.56	3.17
BaO	0.27	0.55	0.36	0.83
MoO_3	0.041	0.007	0.049	0.006
V_2O_5	0.028	-	0.043	-
CoO	0.020	-	0.022	-
NiO	0.040	-	0.060	-
CuO	0.0084	-	0.014	-
ZnO	0.0029	-	0.0056	-
PbO	ND	-	ND	-
TeO_2	0.018	-	0.020	-
SO_3	0.18	-	-	-
CO_2	0.56	-	-	-
NaCl	1.09	-	1.09	-
Active O -110	10.12	-	10.09	-
H_2O	8.81	0.93	8.84	0.94
H_2O+110	8.63	2.94	8.29	3.17
Sum	99.82	100.03	96.41	100.58

All analyses are presented as weight percentages on an air dried basis. A dash indicates no analysis and ND means not detected.

*Sample A (the unfractionated crust) also contains 0.0012% Cr_2O_3.

Table 6. Comparison of elemental analyses of manganese concretions

	Jervis Inlet A	Jervis Inlet B	Baltic Sea Average	Deep Ocean (est. average)	V.S.78
Al	1.70	1.83	1.54	8.57	1.90
Ca	1.33	1.33	1.21	1.57	1.16
Co	.013	.014	.016	0.28	.010
Cu	.0055	.0091	.0048	0.40	.010
Fe	5.01	4.21	22.4	11.7	.86
K	.98	1.03	.076	.68	.96
Mg	1.82	1.83	.57	1.38	-
Mn	32.72	32.82	14.0	19.0	38.9
No	.023	.027	.013	.038	.022
Na	.95	.97	.35	2.08	-
Ni	.026	.038	.075	.58	.045
P	.34	.27	.70	.19	-
Pb	ND	ND	.0038	.10	.025
Ti	.096	.089	.11	.47	.07
Te	.012	.013	-	-	-
Zn	.0019	.0036	.008	0.04-0.40	.023

Jervis Inlet A Discoidal type - Grill, Murray and Macdonald (1968)
B Spheroidal type

Baltic Sea Average - Manheim (1965)
Deep Ocean (estimated average) - Manheim (1965)
V.S.78 (Vermilian Sea) - Mero (1965)

APPENDIX B
ANALYSIS TECHNIQUES AND SUPPLEMENTARY DATA

FIGURES B-1 to B-12

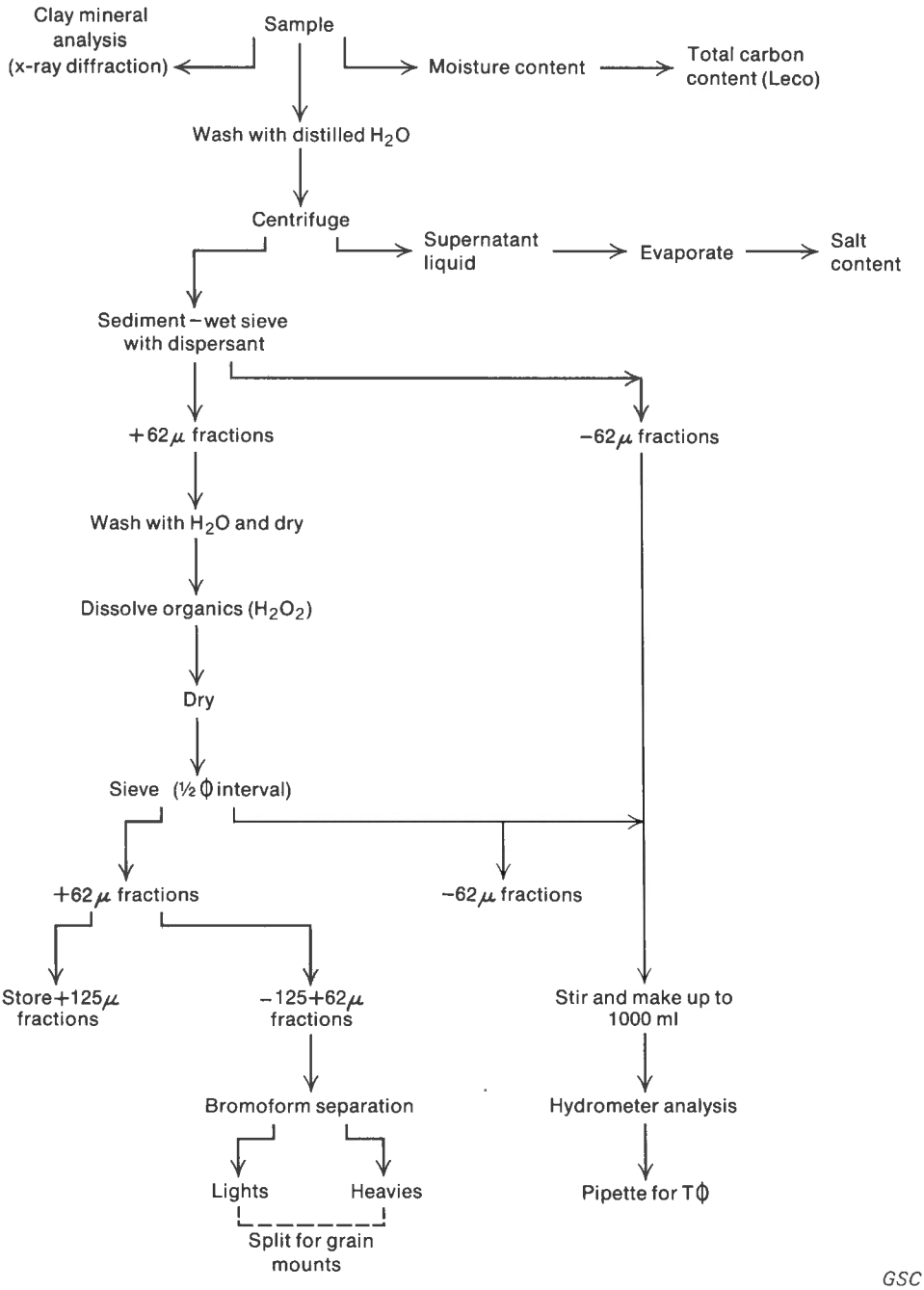

Figure B-1. Procedure for sample analysis.

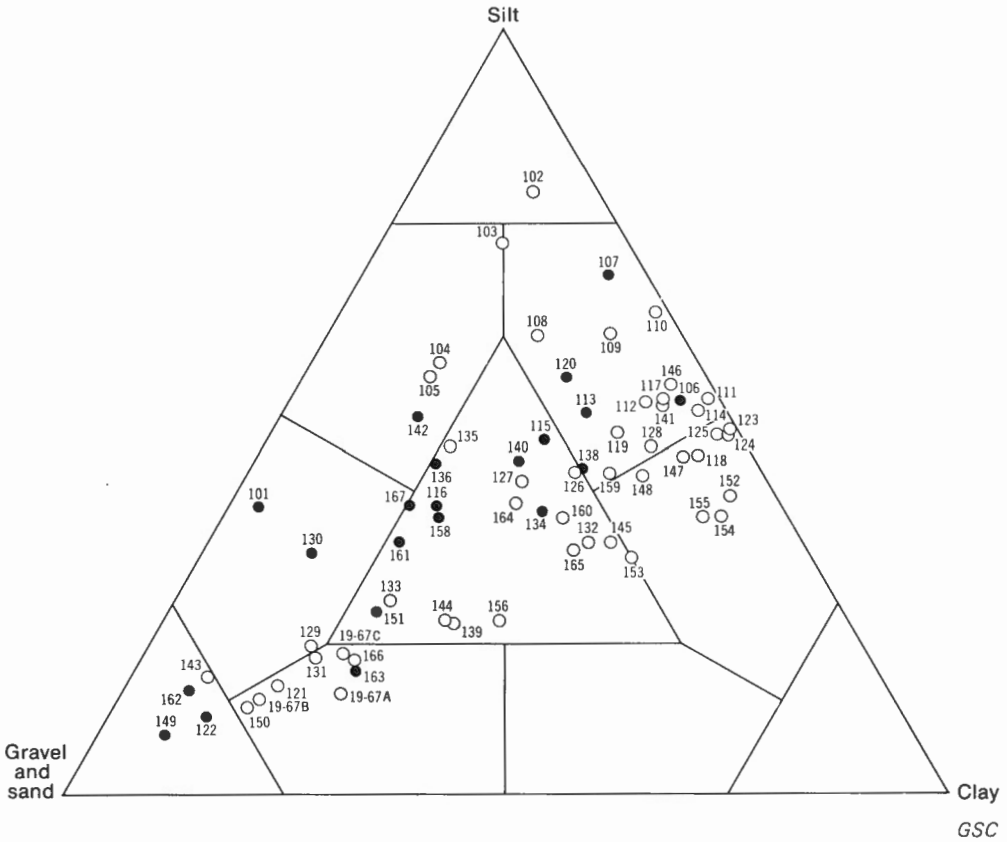

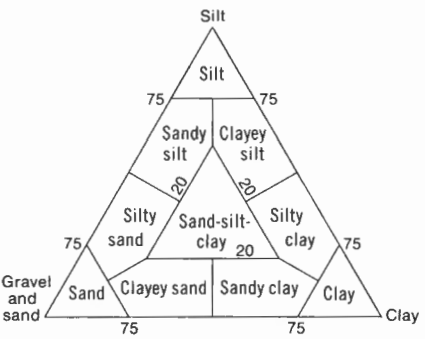

Depth less than 100 fathoms. . . . . ●
Depth greater than 100 fathoms. . . . ○

Figure B-2. Classification of Jervis Inlet sediments according to grain size distribution.

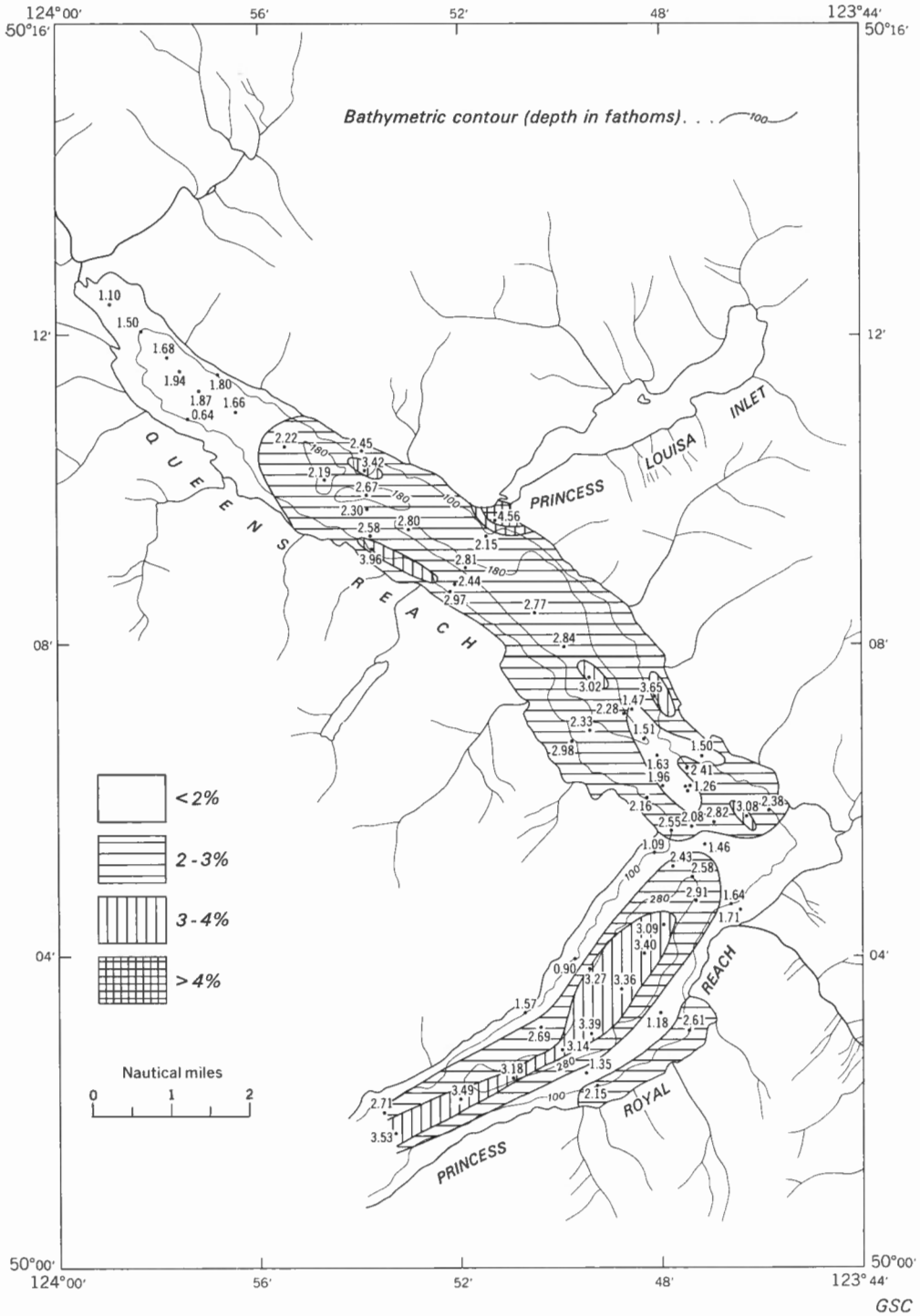

Figure B-3. Total carbon content of sediments in per cent of Jervis Inlet (Northern Portion).

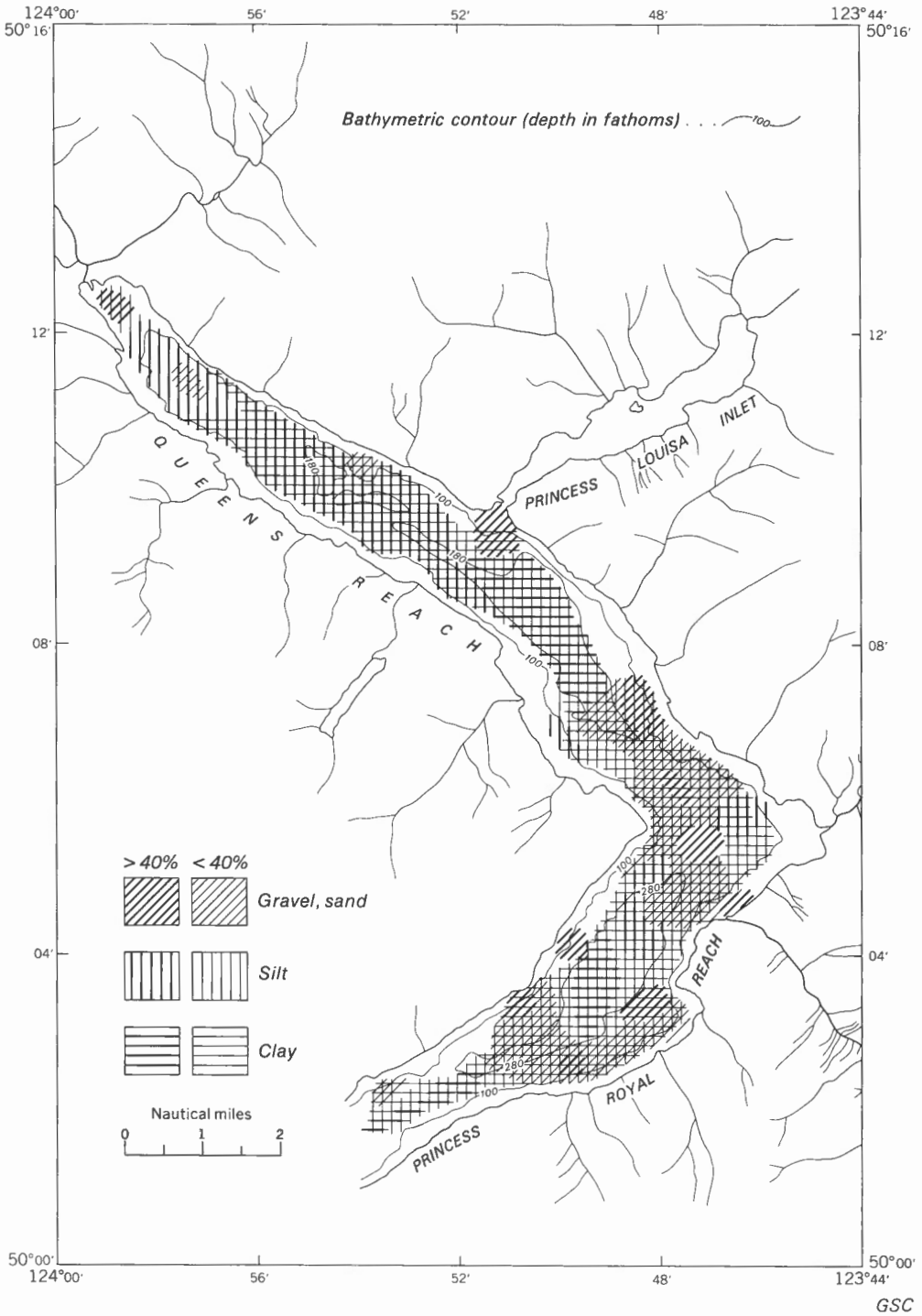

Figure B-4. Sediment-type distribution in Jervis Inlet (Northern Portion).

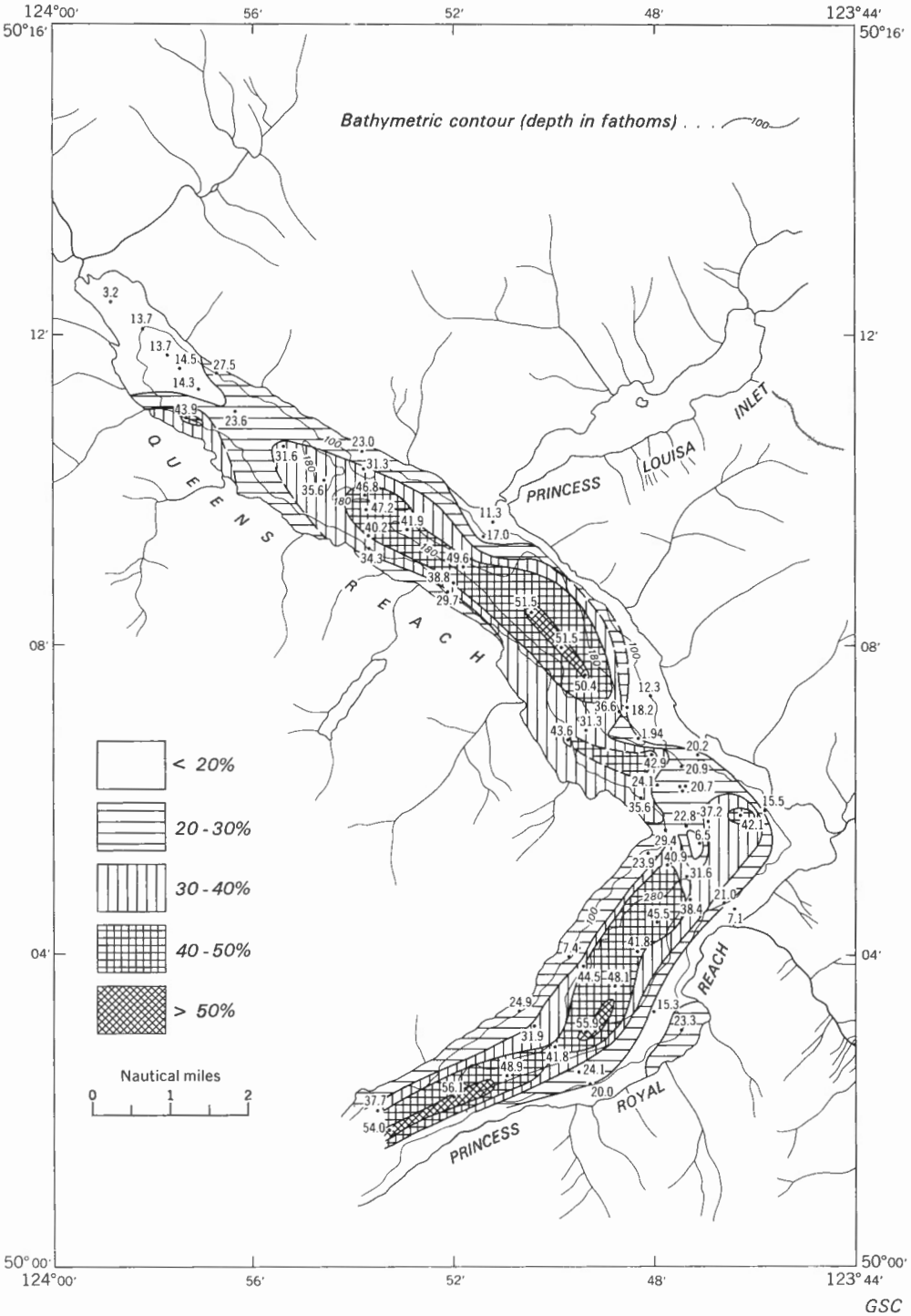

Figure B-5. Clay size particule distribution in upper Jervis Inlet.

Figure B-6. Mean and standard deviation of grain size of surficial sediments along axis of upper Jervis Inlet.

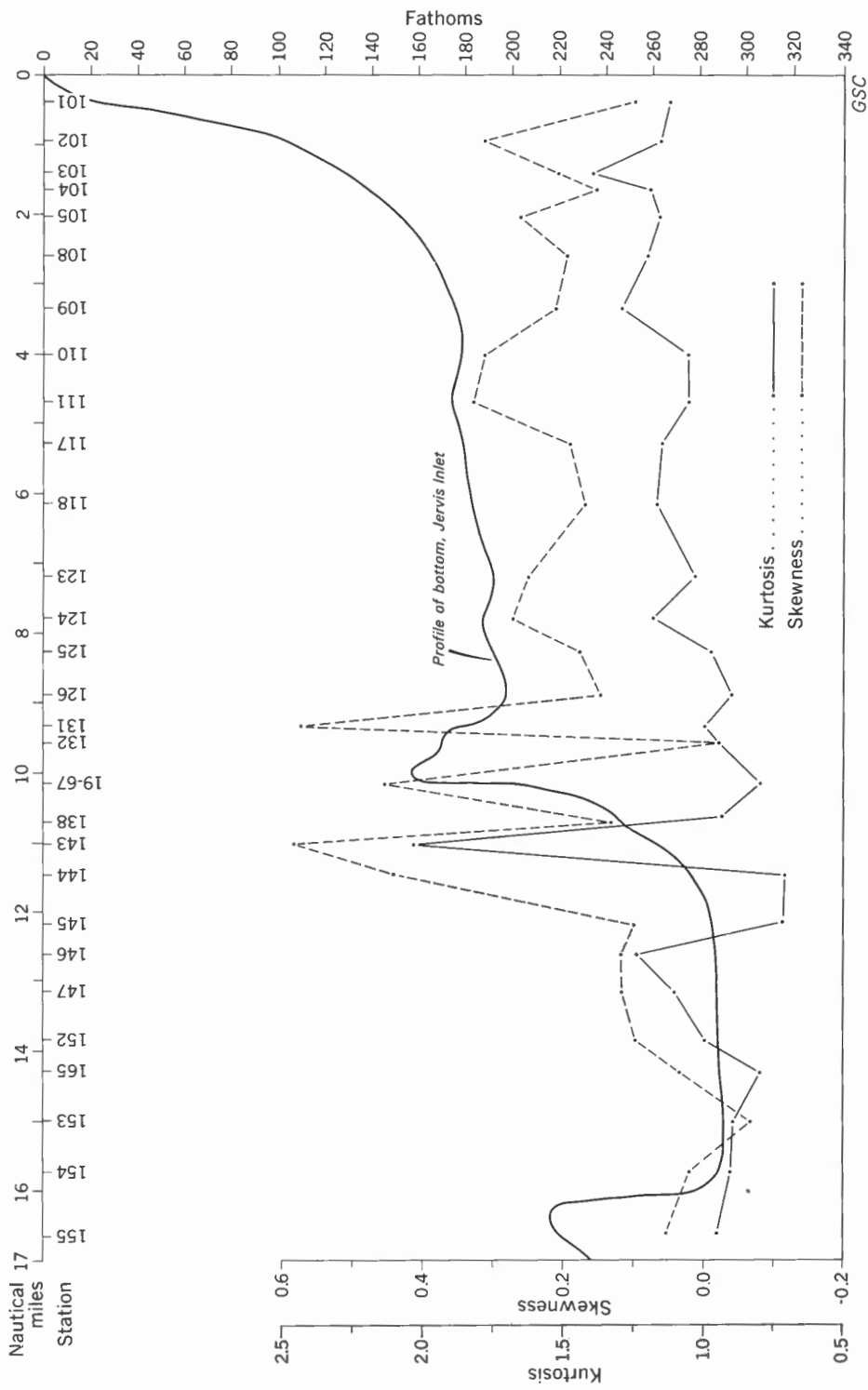

Figure B-7. Kurtosis and skewness parameters of surficial sediments along axis of upper Jervis Inlet.

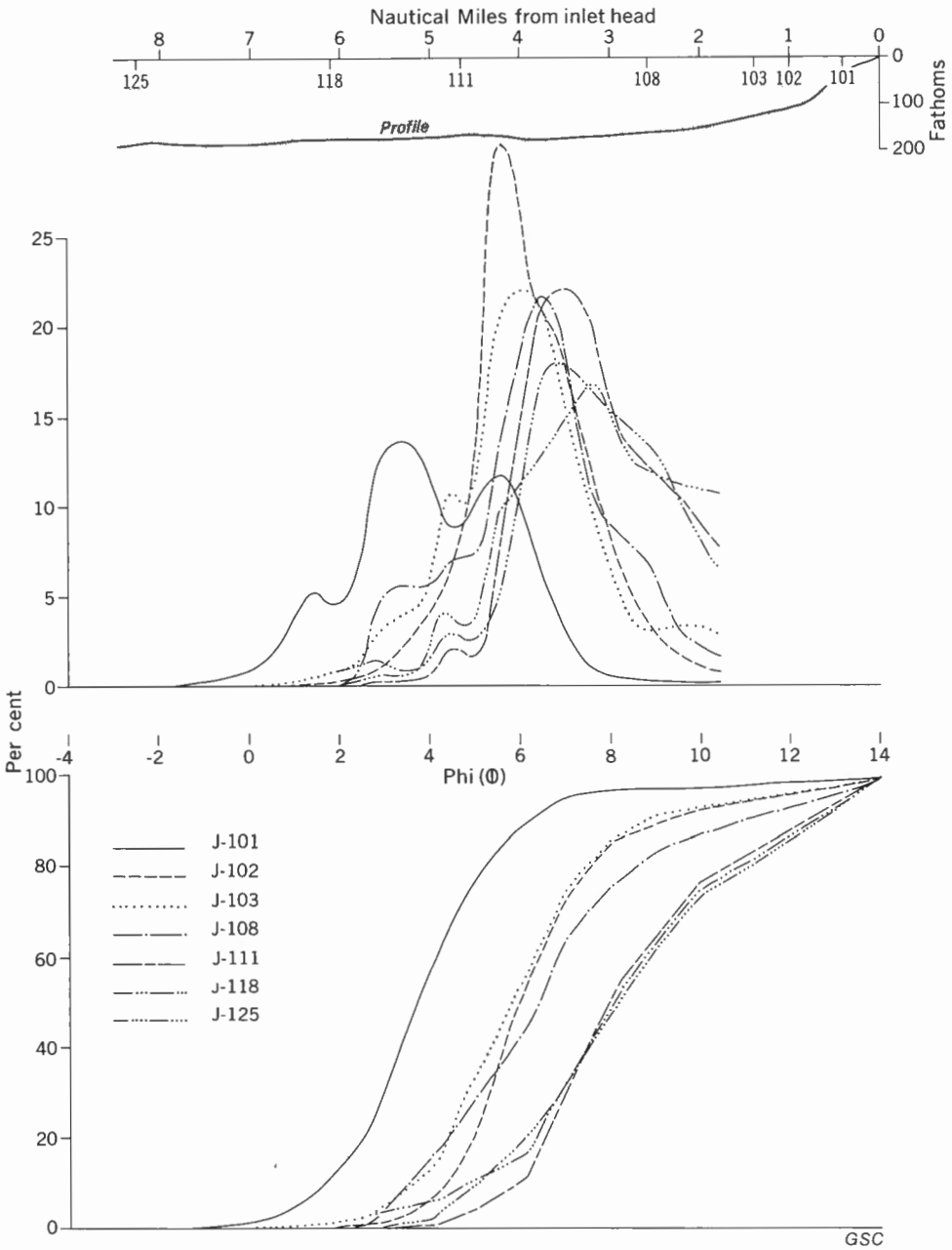

Figure B-8. Longitudinal profile of Queens Reach - cumulative and frequency curves of surficial sediments.

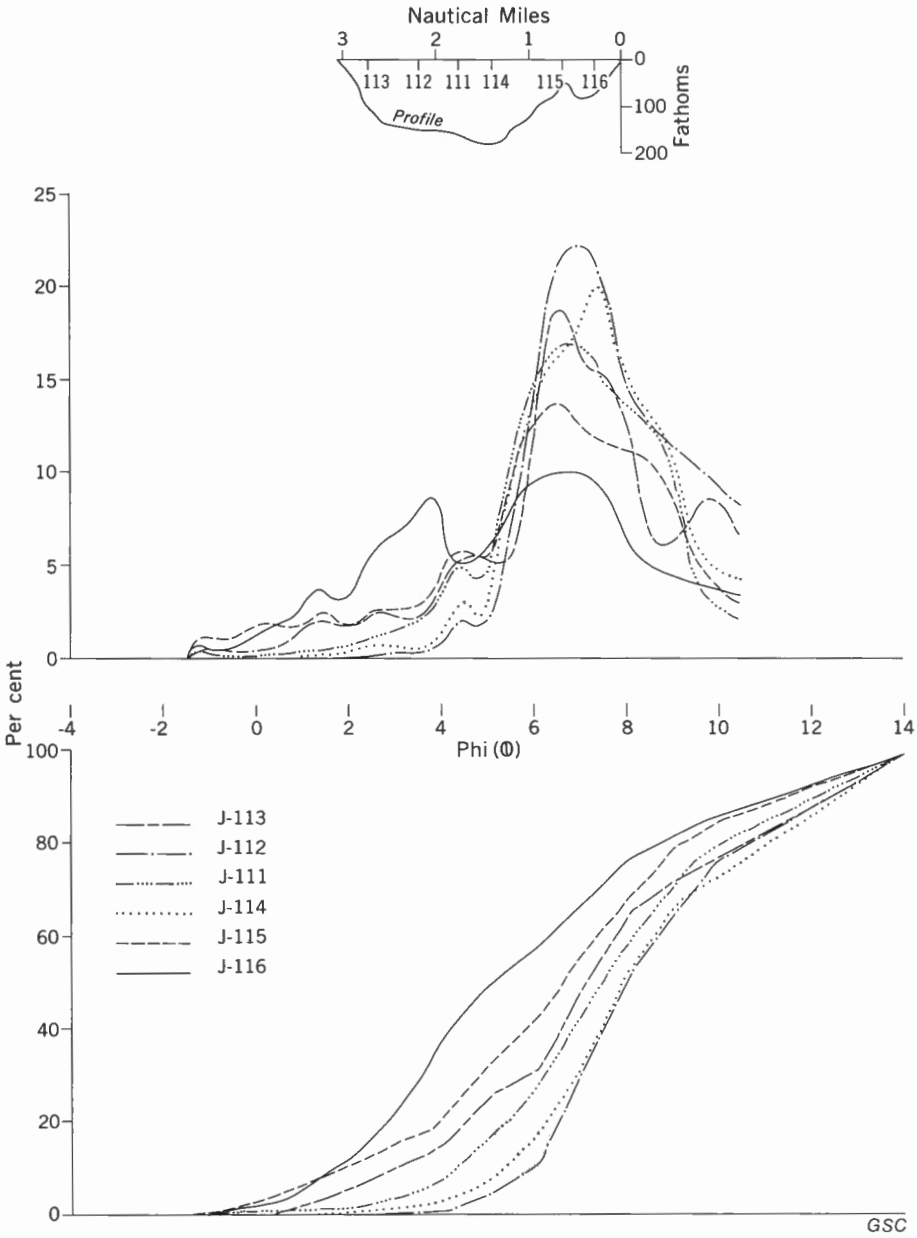

Figure B-9. Transverse profile of Queens Reach – cumulative and frequency curves of surficial sediments.

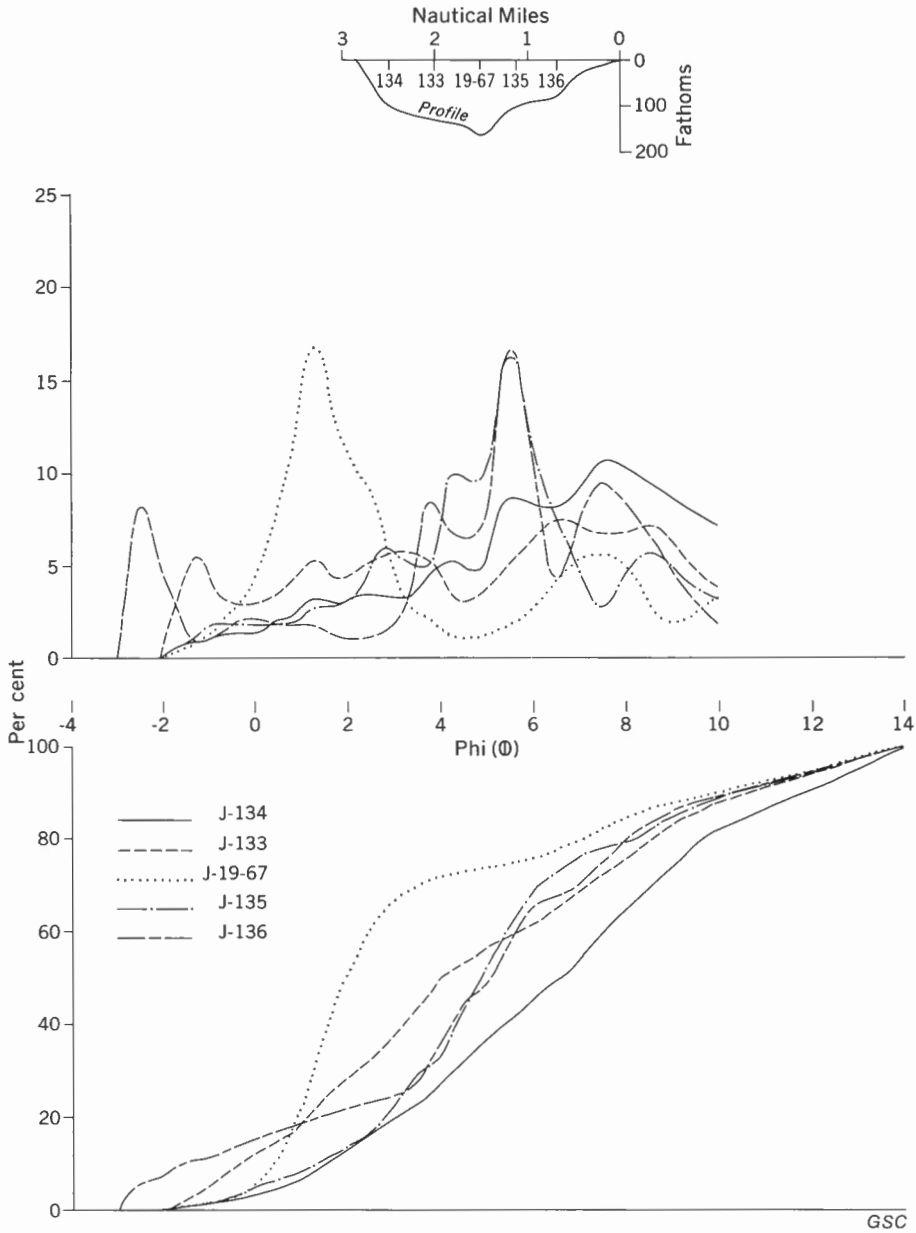

Figure B-10. Transverse section of Queens Reach (over Patrick Sill) – cumulative and frequency curves of surficial sediments.

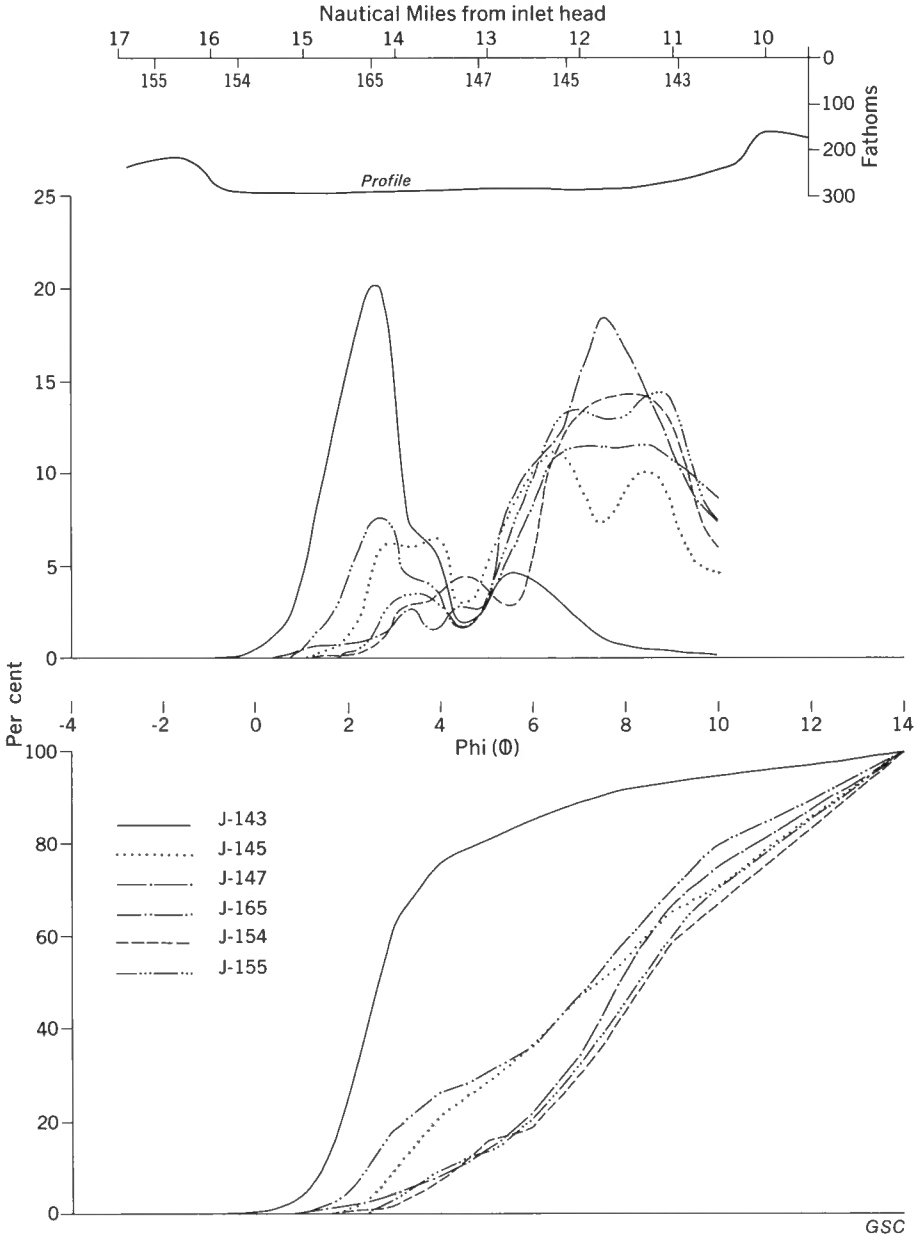

Figure B-11. Longitudinal profile of Princess Royal Reach - cumulative and frequency curves of surficial sediments.

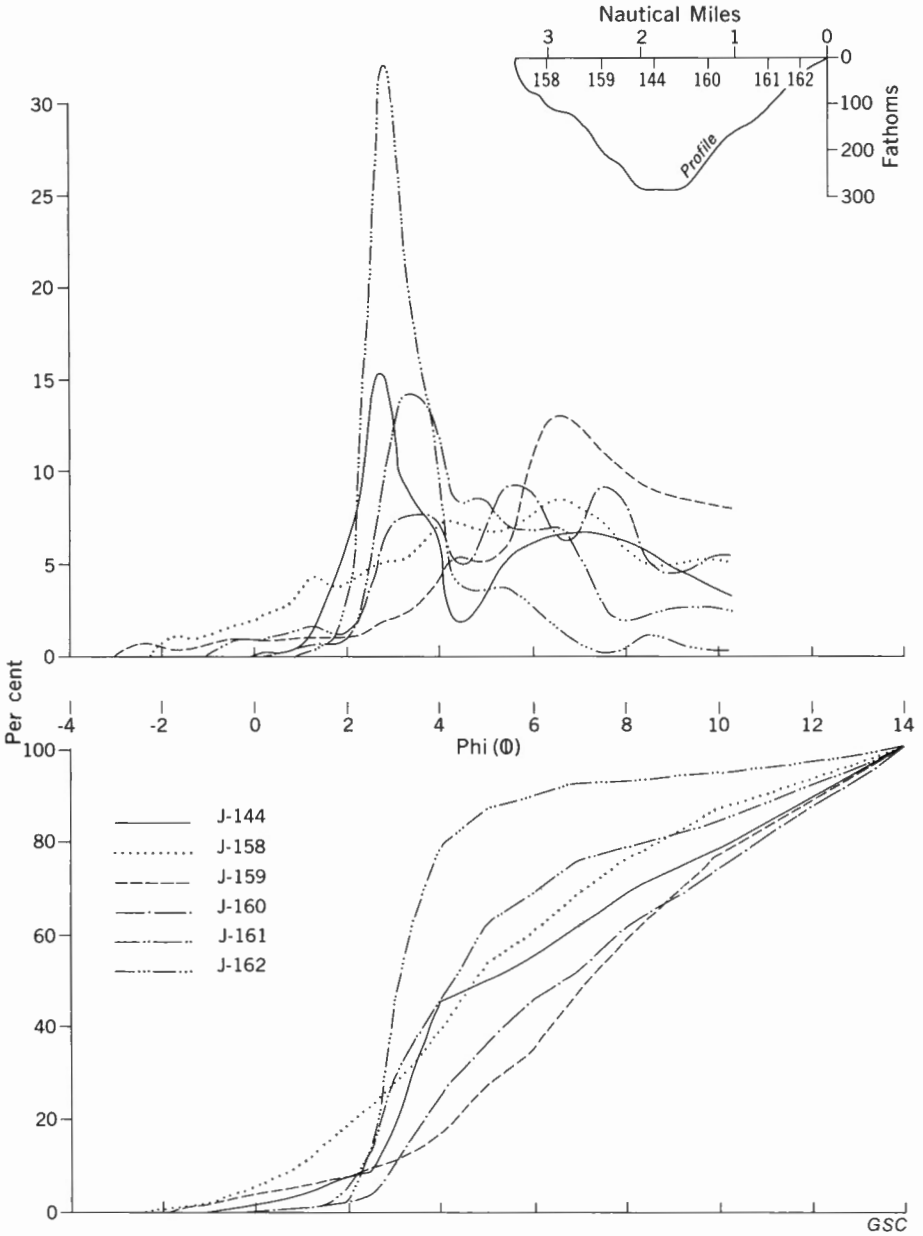

Figure B-12. Transverse profile of Princess Royal Reach – cumulative and frequency curves of surficial sediments.